Egyptian Journal of Zoology (EJZ), Vol. 79: 1-28 (June, 2023) p-ISSN: 1110-6344
Publisher: The Zoological Society of A. R. Egypt e-ISSN: 2682-3160
DOI: 10.21608/ejz.2022.134076.1080

RESEARCH ARTICLE

DIFFERENTIAL STAINING PATTERNS FOR EVALUATION OF OVARIAN AND OVIDUCTS FIBROSIS USING THE POLARIZED LIGHT MICROSCOPE AND THE DIGITAL IMAGES ANALYSIS

Rania A. Ahmed

Zoology Department, Faculty of Science, Suez University, Suez, Egypt

Article History:
Received: 16 April 2022
Revised: 9 June 2022
Accepted: 13 June 2022

Published Online:
12 July 2022

Keywords:
α-SMA
Fallopian tube
Picrosirius red
Van Geison
Vimentin

***Correspondence:**
Rania Ahmed
Zoology Department
Faculty of Science
Suez University
Suez, Egypt
E-mail:
rania.Ahmed@sci.suezuni.edu.eg

ABSTRACT

Several histological and immunohistochemical techniques are used in the diagnosis of fibrosis. To better visualization of collagen fibers in both normal and pathological tissues, new optical approaches are required. The present study aimed to investigate/compare the efficiency of various histological stains, using the traditional light microscope and the light polarizing microscope, to quantify/evaluate the ovarian and oviduct fibrosis induced by high-fat diet (HFD) consumption. Twenty-Four female albino rats (*Rattus norvegicus albinus*) were randomly allotted into 4 groups (n=6): control groups (fed on standard diet for 6 and 12 weeks), HFD1 group (fed on HFD for 6 weeks), and HFD2 group (fed on HFD for 12 weeks). The ovarian and oviduct fibrosis were investigated *via* histological stains including hematoxylin and eosin, Picrosirius Red, van Gieson, and Masson's trichrome stains using traditional light and polarizing light microscopes, in addition to immunohistochemical demonstrations of α-smooth muscle actin (α-SMA) and vimentin. Hydroxyproline and tumor necrosis factor-α (TNF-α) were also investigated biochemically in the ovarian and oviduct tissues. The results showed that the HFD induced ovarian and oviducts fibrosis in time-dependent manner with significant increases in hydroxyproline and TNF-α values, as well as immunoexpression of α-SMA and vimentin. Picrosirius red stain achieved ideal results in collagen demonstration when compared with van Gieson and Masson's trichrome stains. Picrosirius red stain in combination with the polarization microscope represented high sensitivity in collagen estimation in comparison with light microscopy. This work recommended using polarizing microscope as a tool to evaluate fibrosis of both the ovaries and the oviducts.

INTRODUCTION

Fibrosis is the final common pathological result of various organs injuries, ageing, or chronic diseases with multiple causes including inflammatory diseases. Fibrosis is commonly demonstrated in different organs as heart, kidney, lungs, liver, and testis. Without effective treatment, fibrosis impaired organ function and ultimately induces organ malfunction[1-4]. Fibrosis is characterized by excessive scaring formation instead of normal tissue, which then finally

results in the destruction of the tissue architecture and organ remodeling. Scaring is related to multiple causes including increased fibroblasts proliferation, excessive deposition of connective tissue components as extracellular matrix (ECM) proteins, with ECM development influenced by a number of molecular components including transforming growth factor-β (TGF−β), connective tissue growth factor, and epidermal growth factor[1,2,5]. Collagens, elastin, glycoproteins, and proteoglycans are the main components of ECM, which comprise connective tissues and basement membranes. Collagen is the principal structural protein family in connective tissue; it provides structural integrity and regulates the function of tissues through signaling[6,7].

Ovarian fibrosis mainly results by ovarian damage triggered *via* a variety of factors, including high-fat diet (HFD), surgery, aging, inflammation, and immunological disorders. Prior to all body organs, mammalian ovary ages up to decades with marked fibrotic changes[6-8]. A thick capsule, increased mesenchymal connective tissue, and reduced or missing follicles are the key pathological hallmarks of ovarian fibrosis that leads to ovulatory dysfunction[5,9]. However, internationally or nationally, ovarian fibrosis has not attracted much attention[10]. Increased consumption of high-calorie foods in one's daily diet has been shown to cause various fertilization issues and reproductive dysfunction, such as poor oocyte quality, low blastocyst survival rates, abnormal embryonic cellular differentiation, and ovarian apoptosis, in addition to being a dangerous risk factor for cardiovascular disease, diabetes, osteoarthritis, hypertension, cancer, and metabolic disorders[11-13]. HFD is commonly known to associate with polycystic ovary syndrome (PCOS) with its characteristic ovarian fibrosis[14]. Mammalian oviducts, or human fallopian tubes, are an active anatomical region in which all new life in mammalian species begins. It is separated into infundibular, ampullary, isthmic, and intramural segments, which run from the ovarian end to the uterus. Each fallopian tube segment is designed to conduct specific duties that lead to fertilization. The proper structure of each segment of the fallopian tube promotes efficient tubal transfer of ova, sperm, and embryo, which is required for a successful spontaneous pregnancy[15]. The interaction between the ciliary activity of the cells accommodated in mucosal folds and muscle contractions is a sophisticated process that propels gametes and embryos through the oviduct[15]. Due to hormonal influences and ageing, the ECM of the fallopian tubes undergoes many modifications[16]. However, there are not enough studies regarding oviduct fibrosis.

Tissue collagen quantification, in particular, is an essential tool in the clinical diagnosis of fibrosis, as well as in the prediction of outcome and therapy individualization in various organs. Picrosirius red (PSR) and Masson's trichrome (MT) for collagen, silver impregnation for reticulin fibers, orcein staining for elastic fibers, or immunohistochemical stains are commonly used in the histopathological diagnosis of fibrosis. Currently, different microscopes as electron microscopy, bright-field or polarized microscopy are used in evaluation of fibrosis in addition to computer-assisted digital image analysis (DAI) software[17-19]. This study aimed to compare the effectiveness of each of PSR, Van Gieson (VG), and MT stains in quantification of ovarian and oviducts in a rat model for HFD-induced fibrosis using the bright field light microscope and the light polarizing microscope.

MATERIAL AND METHODS

The current study was done following the ethical guidelines for the use and care of laboratory animals and approved with the local ethics committee of Suez University (Approval number: 22319).

Animals and experimental design

Adult female albino rats (*Rattus norvegicus albinus*, n=24, 165-180 g, 10 weeks old)

were purchased from the National Research Center (Giza, Egypt) and were held in clean polypropylene cages with proper ventilation and free access to food and water under standard environmental conditions (22-23°C, 12:12 light/dark cycle, and 62-70% humidity) with free access to food and water. The animals were randomly divided into four groups after one week of acclimatization:

- Control groups: All rats in the control group (n=12) fed standard pellet diet. This group was subdivided into two subgroups: (C1) Rats of this subgroup (n=6) were sacrificed after 6 weeks; (C2) rats of this subgroup (n=6) were sacrificed after 12 weeks.
- HFD1 group: Rats of this group fed on HFD for 6 weeks.
- HFD2 group: Rats of this group fed on HFD for 12 weeks.

HFD was prepared according to Elsisy *et al*.[20].

Sampling and methods

Biochemical analyses of hydroxyproline and tumor necrosis factor-α (TNF-α) in ovary and oviducts

At the end of the experimental periods, all rats were killed by cervical decapitation, and their ovaries and oviducts were dissected out immediately and rinsed with saline. To quantify the collagen content in ovarian and oviducts tissues, tissues were homogenized, and the clear supernatants were separated for hydroxyproline assay as described previously[21]. Furthermore, TNF-α, a common inflammatory indicator, was estimated in ovary and oviducts supernatants using commercially available enzyme-linked immunosorbent assay (ELISA) kit specific for rat TNF-α according to manufacturer's instructions (eBioscience Vienna, Austria, catalogue no: BMS622).

Histological examination

Immediately after killing the animals, specimens of the ovaries and oviducts were fixed in 10% neutral buffered formalin. Thereafter, the specimens were processed for classical histological techniques. Five µm thick sections were cut and subjected to the following histological stains:

- Hematoxylin and eosin stain to examine the histoarchitecture of the ovary and oviducts[22].
- Collagen fiber stains: MT[23], PSR[24], and VG[25].

Immunohistochemical analysis

Following the manufacturer's instructions, the immunohistochemical reactions for α-smooth muscle actin (α-SMA) and vimentin were performed using the avidin-biotin-peroxidase complex method. Briefly, paraffin sections of 4-µm thickness were deparaffinized on charged slides using xylene, and processed for a-SMA and vimentin antibody immunohistochemistry. Tissue sections were rehydrated in descending grades of ethanol series, and rinsed in phosphate-buffered saline (PBS). Endogenous peroxidase activity was blocked by incubating sections in 3% hydrogen peroxide, while nonspecific protein binding was blocked by using a protein block serum-free (Dako, Carpinteria, CA, USA). The sections were incubated for 1.0 hour with the primary antibody against α-SMA (mouse monoclonal anti-α-SMA antibodies; Dako; dilution 1:50) and vimentin (mouse monoclonal anti-vimentin antibody; Dako; dilution: 1:200). Then, slides were incubated with chromogenic 3,3'-diaminobenzidine (Leica Microsystems, Wetzlar, Germany) for 5 minutes, rinsed in tap water, counterstained with hematoxylin, dehydrated, and mounted. All steps were carried out at room temperature as reported previously[26].

Light polarizing microscope examination

At the National Research Center (Giza, Egypt), the MT, PSR, and VG stained sections were examined by an Olympus polarizing microscope BX51-P (Melville, NY, USA) equipped with filters to give circularly polarized illumination in order to assess mature collagen fibrils. After the adaptation of filters to the microscope and the standardization of capture program, the

fields were focused under non-polarized light, and then the polarization was achieved by turning the filter U-POT to an angle of 90º. Birefringence appears during rotation, and the background darkens until it is completely black, and the red and green colors from the birefringence should be very bright. To avoid losing details after polarization, the focus fixed once more[27].

Imaging and morphometric evaluations

To obtain the morphometric data in this study, five MT, PSR, VG, α-SMA, and vimentin stained sections of ovary and oviducts per each rat were examined *via* Olympus light microscope, then five non-overlapping randomly selected fields in each slide of ovary and oviducts were captured at a magnification of 100×. Regarding polarizing microscopy, slides stained with either MT, PSR, or VG were captured with a 40× objective lens, images were recorded on a digital camera (DP11, Olympus), displayed on a high-resolution monitor (Trinitron, Sony Corp, Park Ridge, NJ, USA) and analyzed with SigmaScan Pro image analysis software (SPSS Inc., Chicago, IL, USA).

All digital images obtained from either bright field or polarizing light microscopes were analyzed *via* semi-quantitative scoring system (Image J software, Java based application for analyzing images). The total area of color was measured by adjusting the red color threshold, while excluding the background, and then the red areas were selected and measured to calculate the mean area percentage (%) of each of the following:

- Area (%) of MT, PSR, and VG stained collagen fibers of images obtained from bright field light microscopy in both ovary and oviducts
- Positive immunostained α-SMA area (%) both ovary and oviducts
- Positive immunostained vimentin area (%) in both ovary and oviducts
- Area (%) of MT, PSR, and VG stained collagen fibers in ovary and oviducts of images obtained by polarizing microscopy.

Statistical analyses

The statistical analysis was carried out by one or two-way ANOVA using SPSS, version 25 (IBM Corp. Released 2013). Data were treated as a complete randomization design according to Steel *et al.*[28]. Multiple comparisons were carried out applying least significant difference (LSD) and Duncun test. The significance level was set at $P<0.05$. The correlation between the variables is statistically significant using Pearson Correlation, for significant correlations, significant (2-tailed) will be less than 0.05. Change rate of fibrosis progression was calculated by the formula: [(HFD2 - HFD1) / HFD1] × 100

RESULTS

Hydroxyproline and TNF-α values in ovarian and oviduct tissues of HFD-treated groups

Biochemical determination of hydroxyproline revealed a significant increase in HFD1 and HFD2 groups as compared with their control groups in both ovarian and oviduct tissues. Moreover, HFD2 group showed a significant increase in hydroxyproline values when compared with HFD1 group in both ovarian and oviduct tissues. Concerning TNF-α values, HFD1 group showed a significant increase when compared with C1 group, while HFD2 group showed a significant increase when compared with both HFD1 and C2 groups (Table 1).

Histological results

Hematoxylin and eosin staining findings

Examination of ovarian tissues of the control group stained with hematoxylin and eosin showed the normal histological architecture of the ovary with outer cortex and inner medulla. The ovarian surface epithelium was represented as a single layer of flattened cells with flattened nuclei overlying a thin tunica albuginea layer. The ovarian cortex showed various forms of ovarian follicles in different stages as primary follicles and mature Graafian and corpus lutea, which bulged into the ovarian surface giving it

Table 1: Alterations in hydroxyproline and tumor necrosis factor-α (TNF-α) values in ovary and oviducts tissues among different groups (mean ± standard error).

	Organ	Groups				P value
		C1	HFD1	C2	HFD2	
Hydroxyproline (μg/mg wet tissue)	Ovary	9.99±0.24	32.88±0.62[a]	12.67±0.35	51.57±0.46[b,c]	*P*<0.05
	Oviduct	32.31±0.31	51.19±0.76[a]	36.65±0.39	76.8±0.93[b,c]	*P*<0.05
TNF-α (pg/mg tissue)	Ovary	24.04±0.68	46.81±1.75[a]	24.95±1.16	74.13±1.87[b,c]	*P*<0.01
	Oviduct	42.61±0.57	64.84±1.20[a]	45.99±2.35	123.01±2.15[b,c]	*P*<0.01

C1: control group "1"; C2: control group "2"; HFD1: high-fat diet group "1" treated for 6 weeks; HFD2: high-fat diet group "2" treated for 12 weeks; a: a significant increase when compared with C1 group; b: a significant increase when compared with C2 group; c: a significant increase when compared with HFD1 group.

a lobulated appearance. The ovarian stroma between the follicles was recognized by the presence of fibroblast-like cells, delicate collagen fibers and ground substance. The ovarian medulla revealed richly vascularized loose connective tissue with many relatively large blood vessels in addition to interstitial glandular cells. No histological changes had been observed between the different control subgroups (Figure 1). On the other hand, examination of ovarian tissues obtained from HFD1 group showed loss of normal ovarian histoarchitecture when compared with control group. The ovarian cortex had some degenerated, hemorrhagic, vacuolated, and/or atretic follicles, with distorted corpus luteum having pyknotic nuclei. Some follicle showed marked fatty change. Interstitial stroma and ovarian medulla revealed increase of ECM, which contained dilated and congested blood vessels, edema, and inflammatory cell infiltration. Microscopic examination of ovarian tissues obtained from HFD2 group revealed more advanced histopathological changes by comparing with HFD1. Cystic or degenerate follicles instead of the healthy growing ones were prominent. Oocytes were absent from some follicular cysts. Areas of hemorrhage and edema increased when compared with HFD1. Walls of interstitial stromal cells were apparently thick; the follicles were surrounded by hyperplastic thick fibrous sheath while the ovarian medulla showed hypertrophied fibrous tissues (Figure 1).

Histological examination of sections of oviducts obtained from control group showed that the walls of the oviducts are composed mainly of three layers; mucosa, muscularis, and serosa. Mucosal layer was formed of compact, organized, and prominent longitudinal folds with a central connective tissue lamina propria, lined by simple columnar epithelium, that contained ciliated and secretory epithelial cells. There are also some non-ciliated cells whose apical pole protrudes into the lumen. The middle muscularis was compact and thick, as well as divided into two layers, which are held together by connective tissue; an inner circular layer and an outer longitudinal layer. Serosa appears as a reflection of the peritoneum, which is made up of fibrous tissues that are covered in mesothelium. Several blood vessels were observed as well. A well-shaped tube wall structure with no inflammatory cell infiltration was described as typical tubal histoarchitecture. Histopathological examination of oviducts sections obtained from HFD1 group showed disturbed cellular configurations of epithelial and muscle layers with decreased mucosal folds. The mucosal folds showed a more atrophic appearance with decreased ciliary density. A marked degree of inflammatory cell infiltration was detected, accompanied with congested blood vessels within the tube wall. Submucosal edema was also recorded and/or hyperplasia of the connective tissue

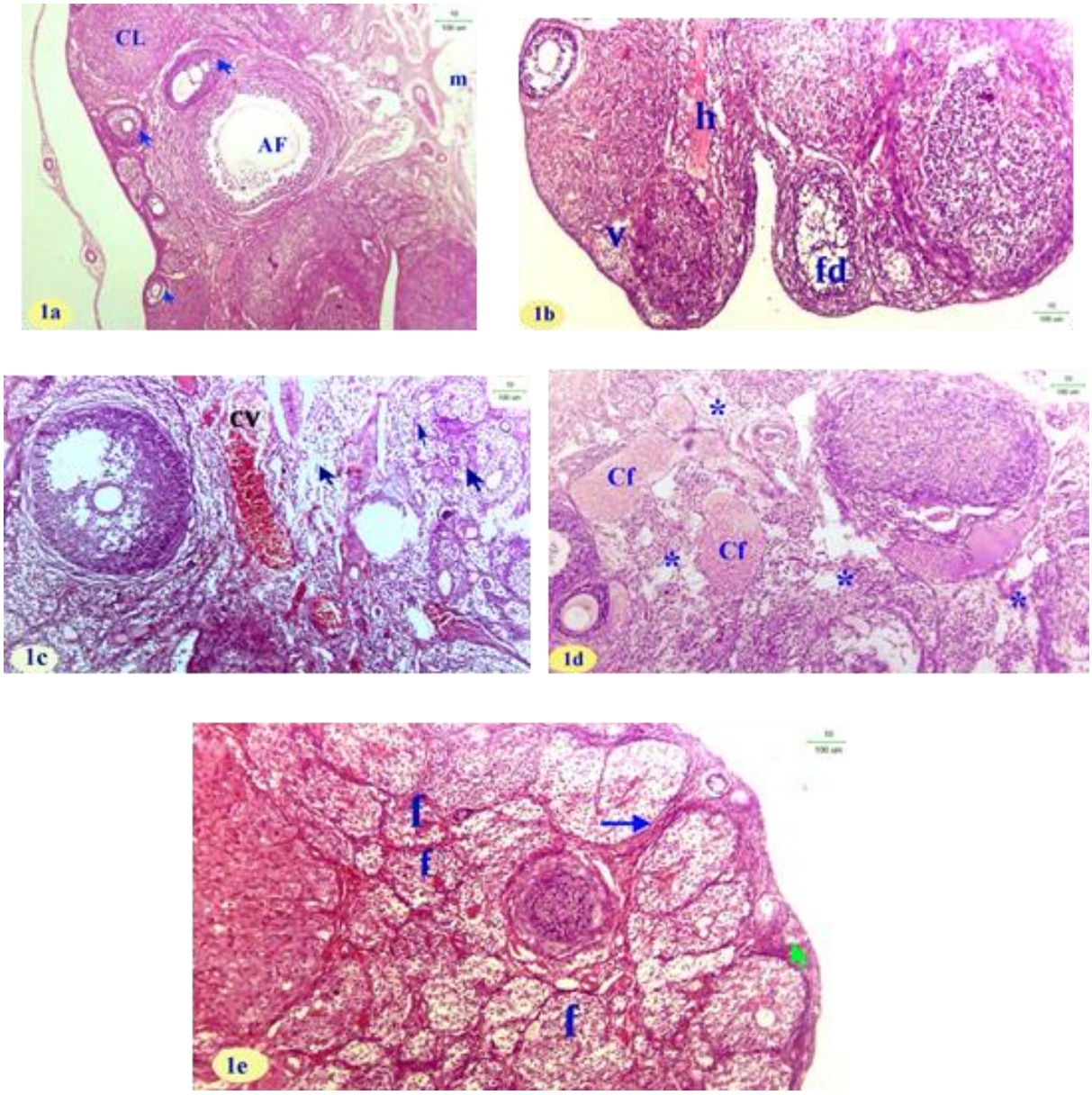

Figure (1): Histopathological alterations in ovary among different groups (hematoxylin and eosin stain; scale bar: 100 µm). **(a)** Section in ovary of a control rat showing normal ovarian medulla (m), and normal cortex including follicles with different degree of maturation (arrows), atretic follicle (AF), corpus luteum (CL). **(b)** Section in ovary of a rat from high-fat diet group "1" (HFD1) group showing cytoplasmic vaculation (v), fatty degeneration (fd), interstitial hemorrhage (h). **(c)** Section in ovary of a rat from HFD1 group, showing congested blood vessel (CV) and interstitial edema with inflammatory cell infiltration (arrows). **(d)** Section in ovary of a rat from HFD2 group showing cystic follicles (CF), and increased ECM accumulation (stars). **(e)** Section in ovary of a rat from HFD2 group showing ovarian fibrosis with many degenerated follicles (f), thickened ovarian capsule (green arrow), and thick bundles of collagen fibers (blue arrow).

and muscularis. Histopathological examination of oviducts sections obtained from HFD2 group showed massive chronic inflammation when compared with both of C2 and HFD1 groups. Obvious occlusive fibrosis and hyalinization with collagen deposits were prominent in the muscularis layer of the thickened tube wall in the majority of sections (Figure 2).

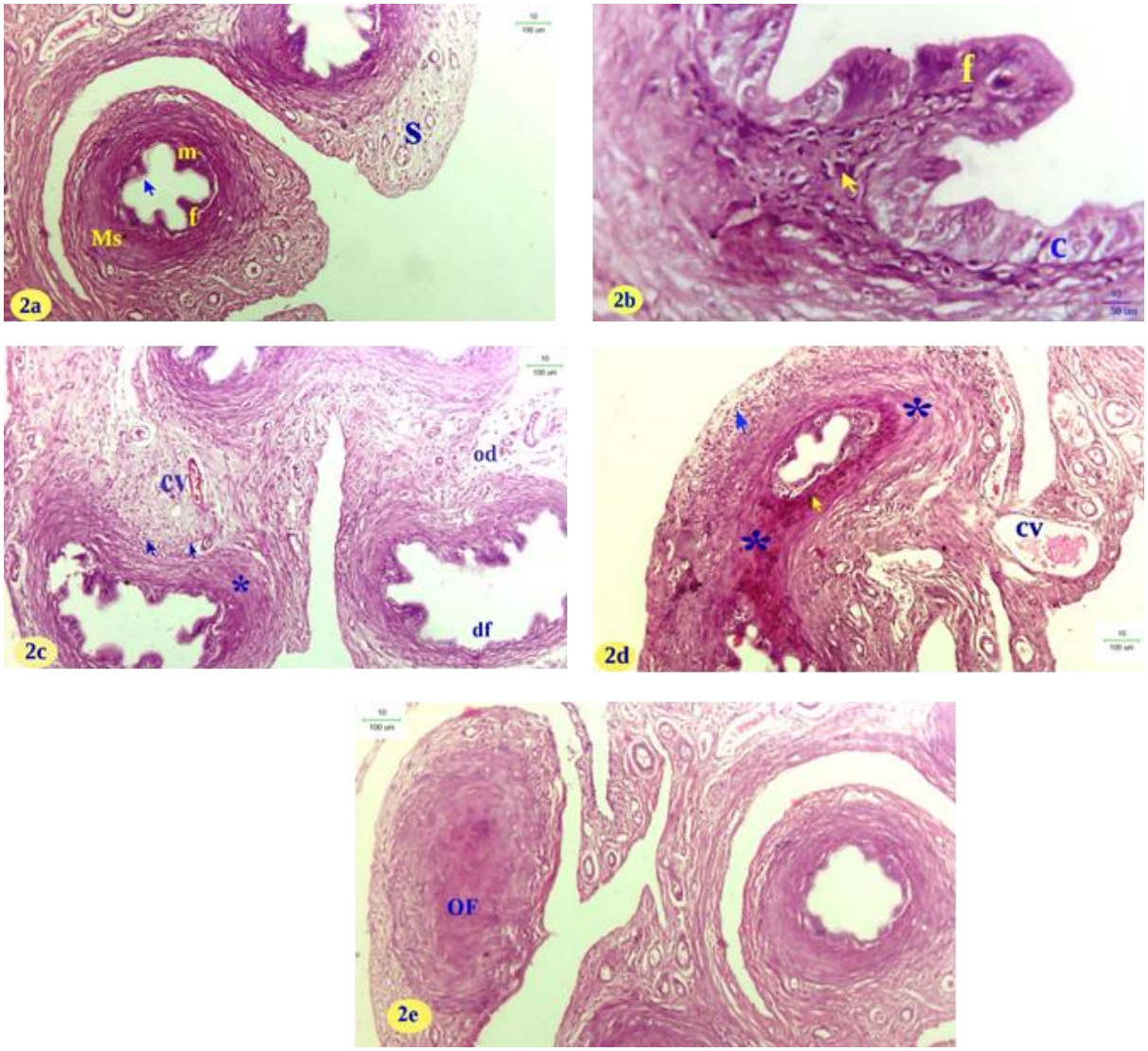

Figure (2): Histopathological alterations in oviducts among different groups (hematoxylin and eosin stain). **(a)** Section in oviduct of a control rat showing well organized and compact oviduct wall that consists of serosa (S), muscularis (Ms), mucosa (m) with mucosal folds covered with ciliated epithelium (arrow) (scale bar: 100 µm). **(b)** Section in oviducts of a control rat in higher magnification showing normal mucosal fold (f), covered with columnar epithelium (c) and housing lamina propria with some inflammatory cells (scale bar: 50 µm). **(c)** Section in oviduct of rat from high-fat diet group "1" (HFD1) group showing degenerated folds (df), congested vessel (cv), moderate thickness of muscularis (star), inflammatory cell infiltration (arrows) and seroal edema (od) (scale bar: 100 µm). **(d)** Section in oviduct of a rat from HFD2 group showing increased thickness of the muscle layer and partial occlusion of oviduct (scale bar: 100 µm). **(e)** Section in oviduct of a rat from HFD2 group showing occlusive fibrosis (OF) (scale bar: 100 µm).

Demonstrations of collagen fibers and fibrosis in in ovary and oviducts of HFD-treated groups

In order to evaluate fibrosis in ovary and oviducts, all sections were stained with MT, PSR, and VG stains. Microscopic examination of ovarian sections stained with each of MT, PSR, and VG revealed that each of the investigated stains achieved an ability to visualize the collagen fibers in all groups. As represented in Figures "3-5", examination of ovaries of control groups demonstrated some collagen fibers as expected because collagen fibers are

normally found in some ovarian structures. Delicate collagen fibers were detected as thin layer of tunica albuginea beneath the surface epithelium, and surrounding follicles and corpora lutea within the ovarian cortex. In the ovarian medulla, collagen fibers appeared within the ground substance with normal density and distribution, and in close association with the vasculature. A slight increase of collagen fibers density was detected by comparing C2 with C1 in MT and PSR stained sections. By comparing with control animals, sections of the HFD1 group revealed marked increase of the collagenous fibers density and distribution within the ovarian cortex and medulla especially around dilated congested blood vessels. Well-developed to thick collagen fibers were observed to capsulate ovarian surface, follicles, and corpora lutea.

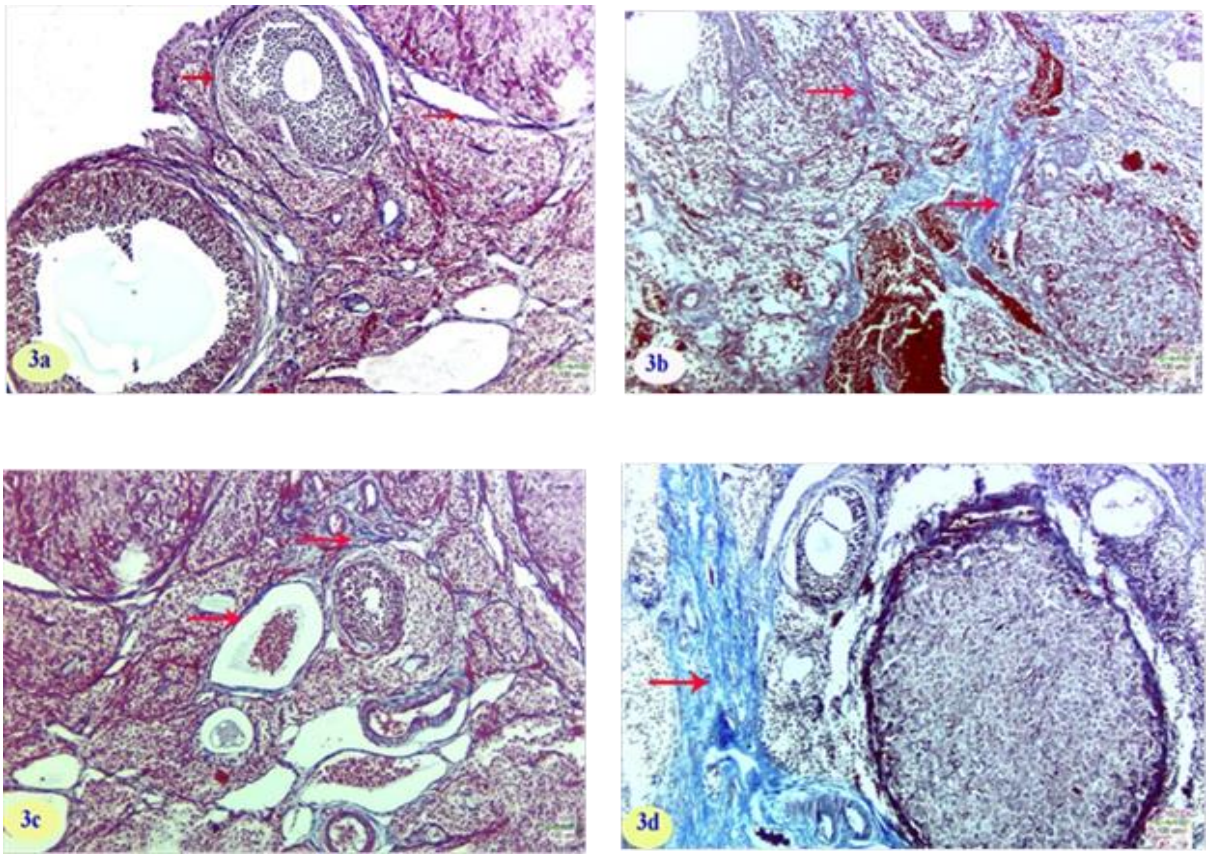

Figure (3): Alterations in collagen contents (arrows) in ovarian tissue (Masson's trichrome stain; scale bar: 100 µm). **(a)** Section in ovary of a control rat showing normal collagen deposition. **(b)** Section in ovary of a rat from high-fat diet group "1" (HFD1) group showing moderate increase of collagen. **(c)** Section in ovary of a control rat from C2 group showing normal collagen distribution. **(d)** Section in ovary of a rat from HFD2 group showing ovarian fibrosis.

Ovaries of HFD2 group had marked increase in the deposition of collagen fibers when compared with HFD1 and control groups. Microscopic examination of ovaries obtained from HFD2 groups showed prominent thick network of intense collagen fibers throughout the ovarian cortical stroma, which proliferated rapidly and continuously into ovarian medulla forming ovarian fibrosis. Some sections stained with PSR showed massive masses of collagenous materials instead of normal ovarian matrix (Figure 4d). However, PSR-stained collagen fibers were more visible and recognizable under the microscope and appeared to be thicker when compared to those stained by MT and VG stained tissues.

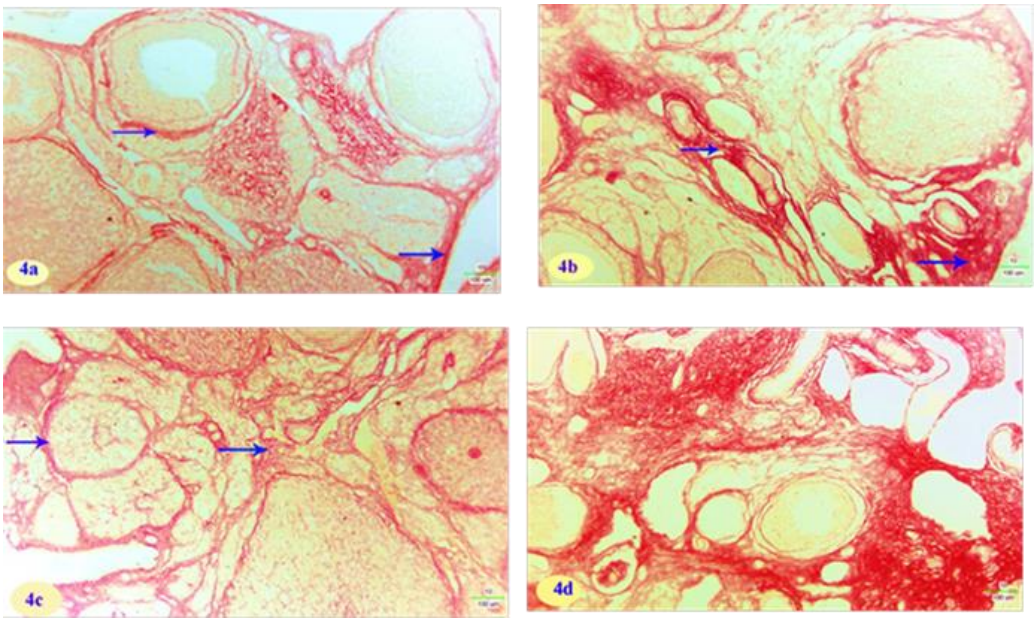

Figure (4): Alterations in collagen contents (arrows) in ovarian tissue in different groups (Picrosirius red stain; scale bar: 100 µm). **(a)** Section in ovary of a control rat showing normal collagen around follicles. **(b)** Section in ovary of a rat from high-fat diet group "1" (HFD1) group showing increased collagen depositions. **(c)** Section in ovary of a control rat from C2 group showing normal collagen distribution. **(d)** Section in ovary of a rat from HFD2 group showing massive amounts of collagenous deposits forming ovarian fibrosis.

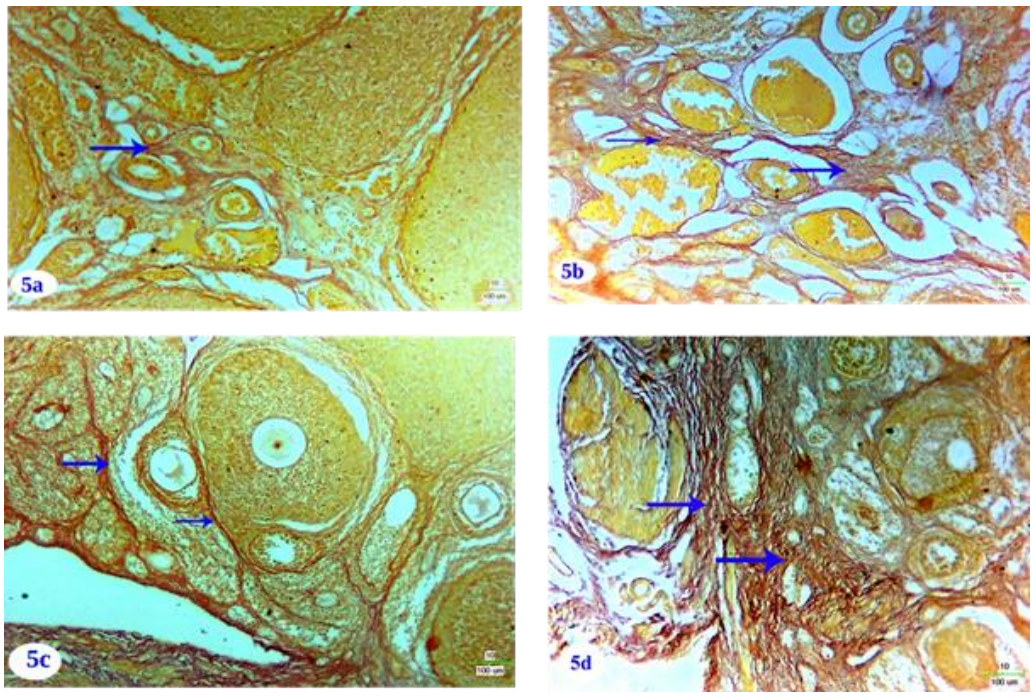

Figure (5): Alterations in collagen contents (arrows) in ovarian tissue among different groups (van Geison stain; scale bar: 100 µm). **(a)** Section in ovary of a control rat showing fine collagen fibers around blood vessels. **(b)** Section in ovary of a rat from high-fat diet group "1" (HDF1) group showing moderate amounts of collagen in ovarian medulla. **(c)** Section in ovary of a control rat from C2 group showing normal collagen distribution around follicles. **(d)** Section in ovary of a rat from HFD2 group showing ovarian fibrosis with thick bundles of collagen fibers.

Analyses of digital images obtained from MT, PSR, and VG stained ovarian sections recorded a significant increase of collagen fibers stained area (%) by comparing (HFD1 and C1), (HFD1 and C2), (HFD2 and C2), (HFD2 and HFD1) groups, respectively. The PSR stain recorded the highest sensitivity to collagen fibers, as there was a significant increase (P<0.05) of collagen fibers stained area (%) in HFD1, C2, and HFD2 groups, when compared with the same groups in each of MT and VG stained sections. In VG stain, there was insignificant difference in collagen stained area (%) by comparing C1 and C2, while MT and PSR stains recorded a significance difference between the same groups (Table 2). The change rate (%) in ovarian fibrosis progression among different groups increased significantly (P<0.05) in PSR stained sections (58.13%), compared to the other two stains "MT (53.43%) and VG (53.09%)".

Table (2): Comparison between effectiveness of Masson's trichrome (MT), Picrosirius red (PSR), and van Gieson (VG) stains in collagen demonstration in ovary of the HFD-treated groups (mean ± standard error).

Time	Groups	Stains			LSD
		MT (%)	PSR (%)	VG (%)	
1	C1	7.87 ± 0.23^{dB}	8.77 ± 0.38^{dA}	8.64 ± 0.44^{cA}	
	HFD1	14.56 ± 0.37^{bB}	29.14 ± 0.78^{bA}	13.28 ± 0.13^{bC}	
2	C2	8.79 ± 0.29^{cB}	9.95 ± 0.24^{cA}	8.82 ± 0.36^{cB}	0.64
	HFD2	22.34 ± 0.52^{aB}	46.08 ± 0.79^{aA}	20.33 ± 0.33^{aC}	
Mean		13.39 ± 1.22^{B}	23.49 ± 3.21^{A}	12.77 ± 1.00^{B}	
LSD			0.73		

C1: control group "1"; C2: control group "2"; HFD1: high-fat diet group "1" treated for 6 weeks; HFD2: high-fat diet group "2" treated for 12 weeks; LSD: least significant difference; a, b, and c: different superscript small letters in each column means a significant difference (P<0.05) between groups within the same staining method; A, B, and C: different superscript capital letter in each raw means a significant difference (P<0.05) among different staining methods.

Concerning collagen demonstration in oviducts, each of MT, PSR, and VG stains showed an ability in demonstrating collagen in control and HFD groups. Examination of the control oviduct sections showed normal collagen density and distribution in oviduct wall. Mucosal layer showed loose connective tissue with a few thin collagen fibers present in the lamina propria of mucosal folds. Muscularis revealed regular amount of collagen fibers interspersed with longitudinal bundles of smooth muscle, also serosa showed moderate amounts of collagen depositions. During examination of oviducts from the HFD1 group, a moderate amount of collagen fibers was detected in the mucosal layer as dense amounts of collagen observed in the lamina propria of mucosal folds. Muscular layer also revealed an increase of collagen fibers in between the two muscle layers, as the muscle fibers were scanty with abundant densely packed collagen fibers in between. Serosa also revealed a marked increase and proliferation of collagen fibers contents. Sections obtained from HFD2 group revealed oviduct fibrosis, as abundant amounts of fibrotic tissue were detected and showed a more condensed pattern and collagen was seen in more quantities with a more disoriented distribution. Several sections of this group showed collagenous materials filling the oviduct lumen forming occlusive fibrosis (Figures 6-8).

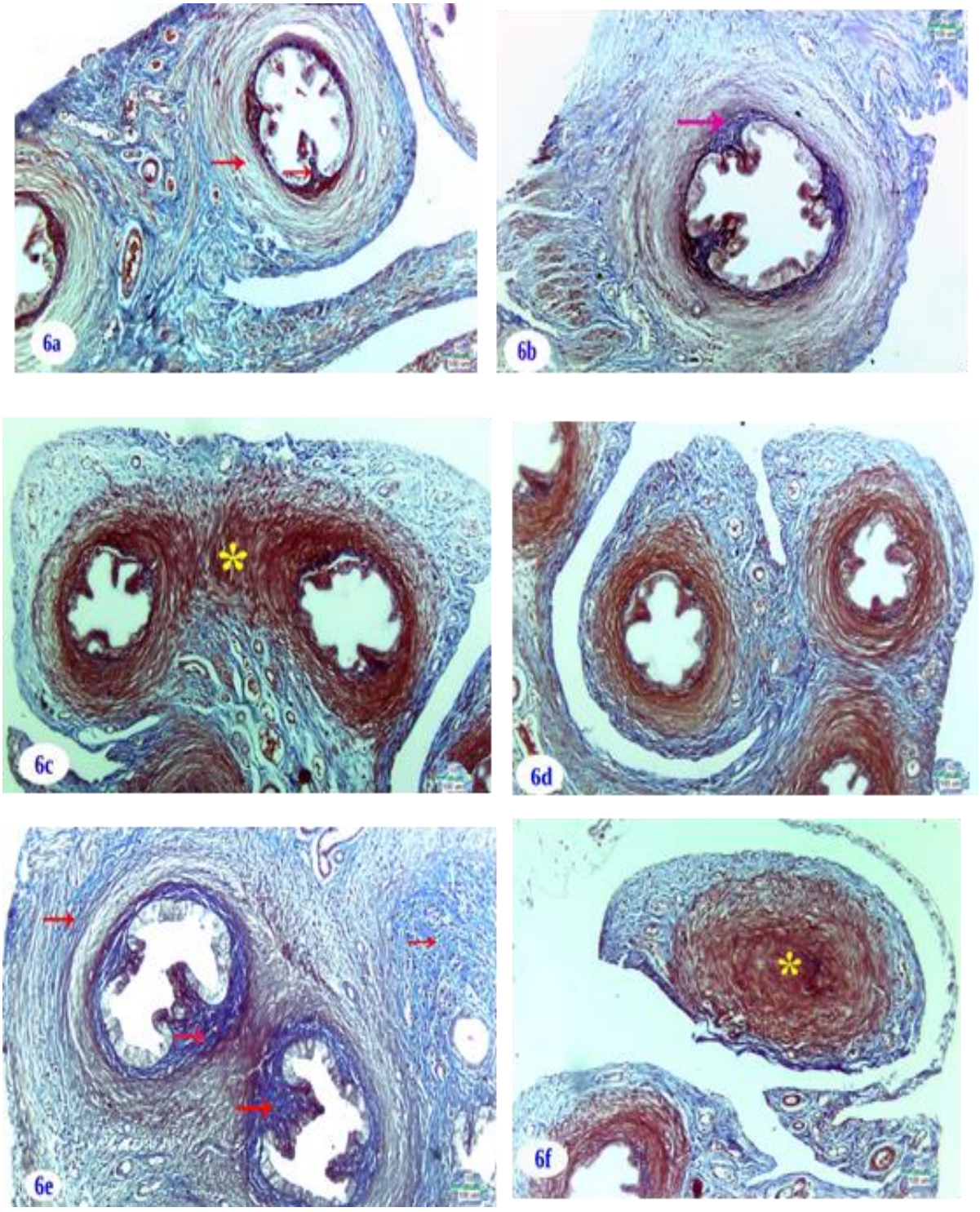

Figure (6): Alterations in collagen contents in oviducts in different groups (Masson's trichrome stain; scale bar: 100 µm). **(a)** Section in oviduct of a control rat showing thin collagen fibers in submucosa and muscularis layers (arrows). **(b)** Section in oviduct of a rat from high-fat diet group "1" (HDF1) group showing increased collagen in the lamina proparia of mucosal folds (arrow). **(c)** Section in oviduct of another rat from HFD1 group showing proliferation of muscle layer (star). **(d)** Section in oviduct of control rat from C2 group, showing normal collagen distribution. **(e)** Section in oviduct of a rat from HFD2 group showing marked increase of collagen in the muscle layer and in the lamina propria of mucosal folds (arrows). **(f)** Section in oviduct of a rat from HGF2 group showing occlusive fibrosis (star).

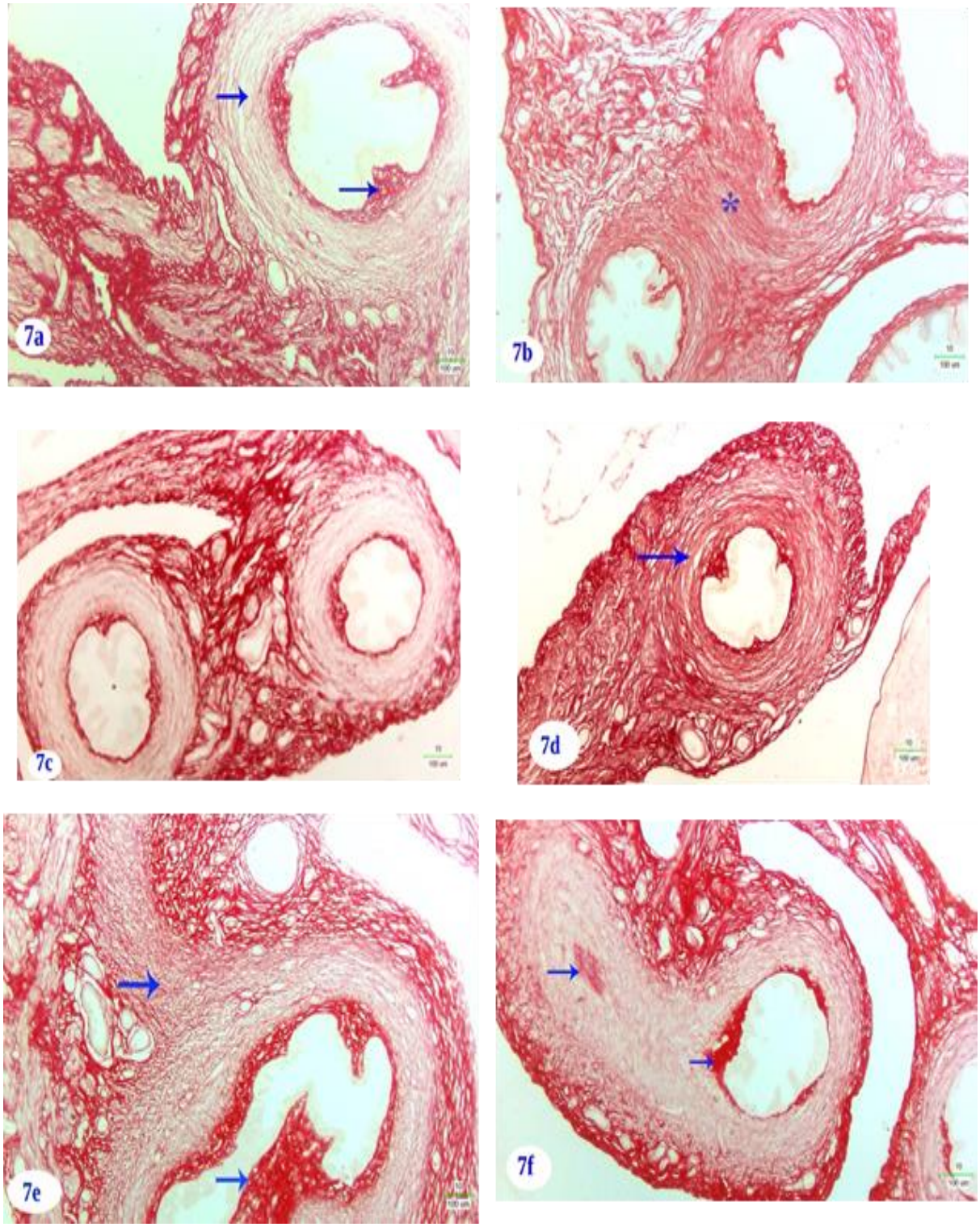

Figure (7): Alterations in collagen contents in oviducts in different groups (Picrosirius red stain; scale bar: 100 µm). **(a)** Section in oviduct of a control rat showing marked collagenous deposits underlying the mucosal folds and thin collagen fibers in submucosa and muscularis layers (arrows). **(b)** Section in oviduct of a rat from high-fat diet group "1" (HDF1) group showing marked collagen in between muscle layers (star). **(c)** Section in oviduct of control rat from C2 group showing normal distribution of collagen fibers. **(d and e)** Sections in oviducts of rats from HFD2 group showing marked increase of collagen in the muscle layer and in the lamina propria of mucosal folds (arrows). **(f)** Section in oviduct of a rat from HGF2 group showing occlusive fibrosis (arrow).

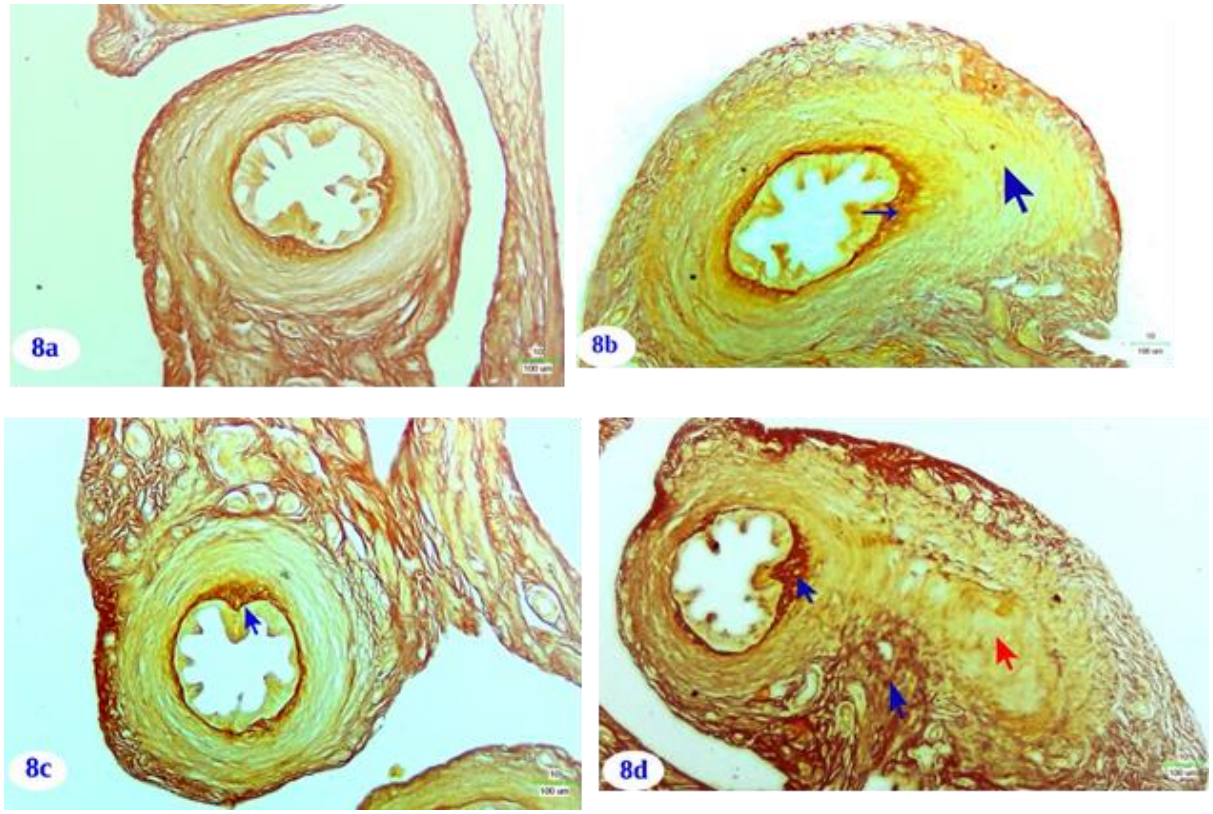

Figure (8): Changes in collagen deposition in oviducts among different groups (van Geison stain; scale bar: 100 µm). **(a)** Section in oviduct of a control rat showing normal collagen deposition in lamina propria. **(b)** Section in oviduct of rat from high-fat diet group "1" (HDF1) group showing mild increase of collagen fibers in lamina propria and increased thickness of muscularis (arrows). **(c)** Section in oviduct of control rat from C2 group showing normal distribution of collagen fibers. **(d)** Section in oviduct of a rat from HFD2 group occlusion of oviduct *via* fibrosis (red arrow) and increased sub mucosal collagen (blue arrow).

By comparing each of MT, PSR, and VG stained sections, within the same group; microscopic examination showed collagen fibers highlighted more clearly visualized by PSR staining, which allowed detecting higher amounts and collagen fibers, as compared with MT VG stains. Digital image analyses revealed that each of MT, PSR, and VG stains visualized a significant increase of collagen fibers stained area (%) between each of (C1 and C2), (HFD1 and C1), (HFD2 and C2), and (HFD2 and HFD1), respectively. Sections stained by PSR recorded a significant increase of collagen (%) between C2 and C1 groups, where there was insignificant difference between these groups within MT and VG stained sections. Moreover, by contrast to MT and PSR stains, VG stained section revealed insignificant difference between C2 and HDF1 groups (Table 3). The change rate (%) in oviduct fibrosis progression among different groups increased significantly (P<0.05) in PSR stained sections (51.98%), compared to the other two stains "MT (35.73%) and VG (33.89%)".

Correlation between hydroxyproline values and MT, PSR, and VG stained collagen

The statistical analyses revealed a significant correlation (P<0.05) between hydroxy-proline values, and fibrosis (%) stained with each of MT, PSR, and VG stains in both ovarian and oviducts tissues. The highest correlation was recorded with the PSR in ovary (0.996) and oviduct (0.995), followed

Table (3): Comparison between effectiveness of Masson's trichrome (MT), Picrosirius red (PSR), and van Gieson (VG) stains in collagen demonstration in oviducts of the HFD-treated groups (mean ± standard error).

Time	Groups	Stains			LSD
		MT (%)	PSR (%)	VG (%)	
1	C1	17.89 ± 0.39^{dB}	19.33 ± 0.44^{dA}	18.03 ± 0.60^{cB}	
	HFD1	23.82 ± 0.25^{bB}	29.22 ± 0.33^{bA}	19.59 ± 0.34^{bC}	
2	C2	19.23 ± 0.20^{cB}	20.05 ± 0.41^{cA}	19.41 ± 0.21^{bB}	0.53
	HFD2	32.33 ± 0.50^{aB}	44.41 ± 0.34^{aA}	26.23 ± 0.30^{aC}	
Mean		23.32 ± 1.19^{B}	28.25 ± 2.12^{A}	20.81 ± 0.69^{C}	
LSD			0.61		

C1: control group "1"; C2: control group "2"; HFD1: high-fat diet group "1" treated for 6 weeks; HFD2: high-fat diet group "2" treated for 12 weeks; LSD: least significant difference; a, b, and c: different superscript small letters in each column means a significant difference ($P<0.05$) between groups within the same staining method; A, B, and C: different superscript capital letter in each raw means a significant difference ($P<0.05$) among different staining methods.

by the MT in ovary (0.981) and oviduct (0.987), and the VG in ovary (0.978) and oviducts (0.927), which may indicates the higher efficiency and accuracy of PSR stain in fibrosis diagnosis by analogy with the biochemical estimation of hydroxyproline in ovary and oviducts.

Evaluation of fibrosis by polarizing microscope

In order to examine the efficiency of polarizing microscopy in determination of ovarian and oviduct fibrosis, each of MT, PSR, and VG stained slides of both ovary and oviduct, were examined with polarizing microscopy. Both MT and VG stained section did not detect any polarization in both ovary and oviducts, thus, MT and VG stained slides were excluded from the current polarizing microscopy study (Figure 9). The polarizing microscopy achieved high visualization of fibrosis in PSR stained sections in both ovary and oviducts. The PSR stained sections were further analyzed using polarized light microscope in order to determine the maturity of collagen within the tissue of ovary and oviducts. Under polarized light, the hue of collagen indicates its maturity, which ranges from green to yellow to red.

In ovary, PSR-stained slides obtained from C1 group showed delicate collagen fibers in yellowish green color. Examination of PSR-stained slides obtained from HFD1 group showed significant increase of collagen fibers in yellowish green and orange red color when compared with control group. Sections obtained from C2 group revealed thin red collagen fibers in ovarian tissues. The HFD2 slides revealed ovarian fibrosis as thick bundles and massive masses of collagenous material with mixed colors, yellowish green and orange red were detected (Figure 10, Table 4).

Concerning oviducts, control PSR-stained slides revealed normal orange red collagen content in oviduct wall. The HFD1 group showed increase in newly formed yellowish green collagen fibers when compared with control group. C2 showed slight increase of green immature collagen fibers when compared to C1. HFD2 showed oviduct fibrosis, with significant increase of red thick mature collagen fiber in oviduct wall, as well as marked accumulation of immature green collagen fibrils that completely occluded the oviduct lumen (Figure 11, Table 5).

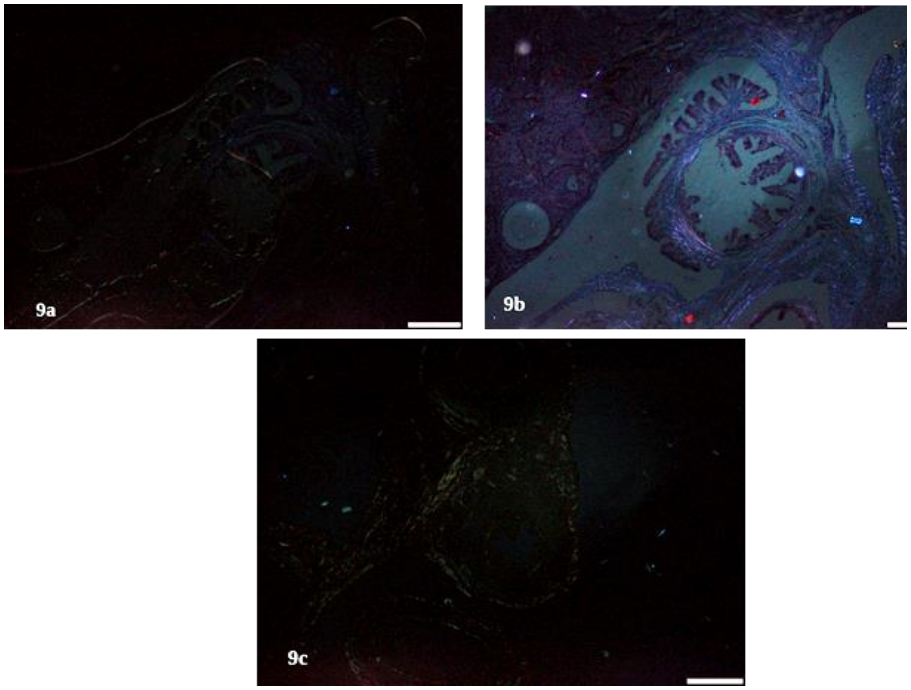

Figure (9): Sections in ovary and oviducts showing no polarization with Masson's trichrome stain with black filter **(a)** or gray filter **(b)**. **(c)** Section of oviduct stained with van Geison stain showing no polarization (scale bar: 50 µm).

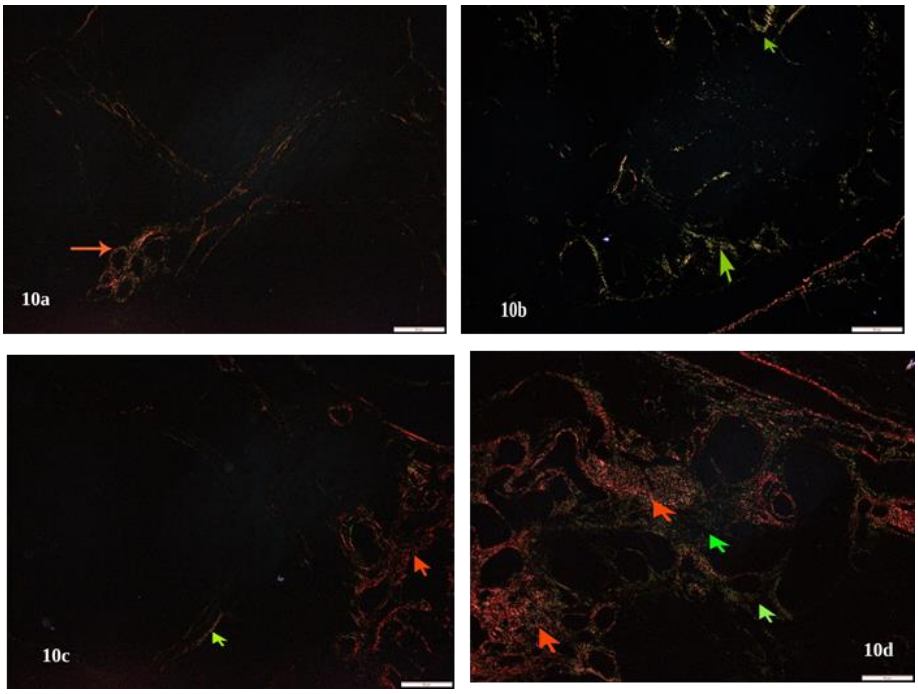

Figure (10): Examination of Picrosirius red-stained ovarian sections by polarizing microscope (scale bar: 50 µm). **(a)** Section in control rat showing thin mature collagen type I around vessels (orange arrow). **(b)** Section in rat from high-fat diet group "1" (HDF1) group showing accumulation of immature yellowish green collagen fibril (green arrow). **(c)** Section in control rat from C2 group showing normal mature red collagen (orang arrow) and mild increase of immature green fibrils (green arrow). **(d)** Section in rat from HFD2 group showing massive amounts of red mature (orang arrow) and green immature (green arrow) collagens.

Table (4): Comparison between light and polarizing microscopes in evaluation of ovarian fibrosis among high-fat diet groups (mean ± standard error).

Period (week)	Microscopes		Mean
	Light	Polarizing	
0	9.36 ± 0.31^{cA}	3.47 ± 0.13^{cB}	6.42 ± 0.90^{c}
6	29.14 ± 0.78^{bA}	6.98 ± 0.18^{bB}	18.06 ± 3.36^{b}
12	46.08 ± 0.79^{aA}	17.87 ± 0.34^{aB}	31.97 ± 4.27^{a}
Mean	23.49 ± 3.21^{A}	7.95 ± 1.24^{B}	
Change (%)	58.13%	156.02%	

a, b, and c: Different superscript small letters in each column means a significant difference (P<0.05) between groups within the same microscope investigation; A, B, and C: different superscript capital letter in each raw means a significant difference (P<0.05) among the light and polarizing microscopes.

Comparison between PSR-stained sections in light and polarizing microscopy

As expected, by comparing data obtained from digital images analyses of each of PSR stained section that captured by light and polarizing microscopes, it was found that the change rate (%) of fibrosis progression recorded by polarizing microscope is more sensitive in ovarian and oviducts fibrosis evaluation than those of light microscope. In ovary, fibrosis change rate recorded (156.02%) by polarizing microscope when compared with that recorded by light microscope (58.13%), which means a 2.5 folds increase. Regarding oviducts, by comparing the change rate of fibrosis progression between PSR-stained section by light and polarizing microscopes, it was revealed that the polarizing microscope recorded "88.43%" when compared with that of light microscope (51.98%), which is equivalent to 1.7 folds increase (Tables 4 and 5).

Immunohistochemical demonstration of α-SMA and vimentin in in ovary and oviducts of HFD-treated groups

Analyses of image obtained from α-SMA and vimentin stained sections of ovary and oviducts revealed a significant difference in α-SMA and vimentin (%) stained area between all groups in both ovarian and in oviducts tissues. The value of α-SMA increased significantly in HFD1 group when compared with C1 group, and in HFD2 group when compared with the C2 and HFD1 groups in both ovarian and oviduct tissues (Table 6; Figures 12 and 13).

Regarding vimentin immunoexpression, the situation was not much different from the α-SMA, a significant increase was recorded in vimentin by comparing HFD1 and control, as well as HFD2 with HFD1 and C2. However, there was a significant increase in vimentin (%) stained areas in C1 rats by comparing with those of C2 (Table 6; Figures 14 and 15).

DISCUSSION

Based on the considerations of the lack of comparative histological studies on fibrosis of ovary and oviducts, we deemed it interesting to perform a comparative image analysis of three known conventional histological staining methods, MT, PSR, and VG stains, in terms of their sensitivity to demonstrate and quantify collagen fibers and fibrosis in formalin-fixed paraffin-embedded sections of ovary and oviducts using computer-aided morpho-metric image analysis in normal light and polarizing microscopy. Immunohisto-chemical demonstrations of α-SMA, in addition to biochemical estimation of hydroxyproline (the main component of collagen) and TNF-α in both ovarian and oviduct tissues was determined.

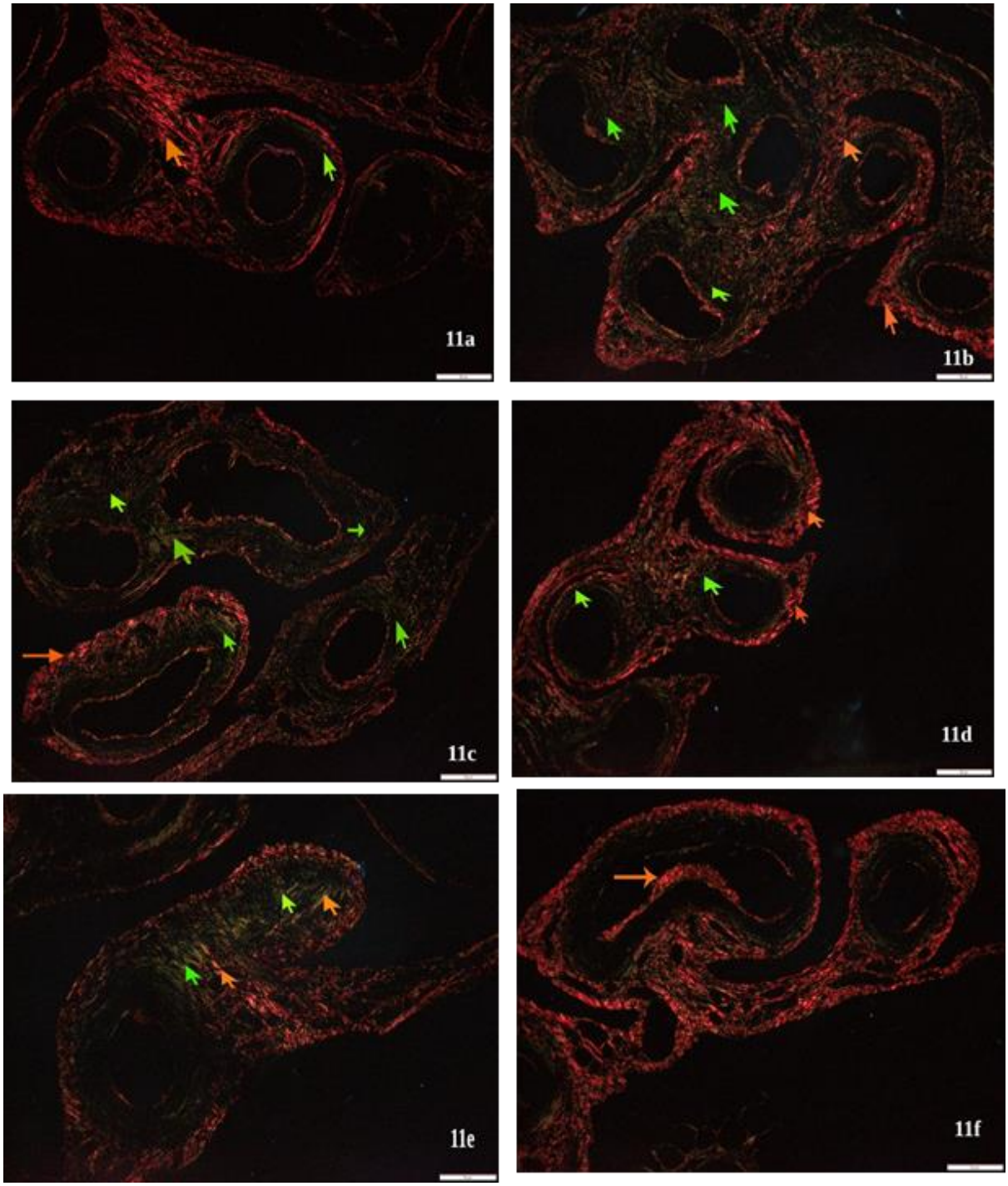

Figure (11): Examination of Picrosirius red-stained oviducts sections by polarizing microscope (scale bar: 50 µm). **(a)** Section in control oviduct showing normal amounts of red mature collagen (orange arrow) and fine immature yellowish green collagen fibril (green arrow) infiltrated the muscularis layer. **(b and c)** Sections from rats from high-fat diet group "1" (HDF1) group showing proliferation and increase of immature yellowish green collagen fibers (green arrows) with increase in red mature collagen. **(d)** Section in a control rat from C2 group showing normal distribution of red collagen in oviduct wall with slight increase of immature collagen fibers by comparing with control sections from C1 group. **(e)** Section in oviduct of a rat from HFD2 group showing accumulations of mature and immature green collagen in oviduct lumen casing occlusive fibrosis. **(f)** Section in oviduct of another rat from HFD2 group showing significant increase of mature collagen.

Table (5): Comparison between light and polarizing microscopes in evaluation of oviduct fibrosis among high-fat diet groups (mean ± standard error).

Period (week)	Microscopes		Mean
	Light	Polarizing	
0	19.69±0.4^{cA}	8.31±0.16^{cB}	14.00±1.73^{c}
6	29.22±0.33^{bA}	13.05±0.42^{bB}	21.14±2.45^{b}
12	44.41±0.34^{aA}	24.59±0.65^{aB}	34.50±3.01^{a}
Mean	31.11±2.48^{A}	15.32±1.68^{B}	
Change (%)	51.98%	88.43%	

a, b, and c: Different superscript small letters in each column means a significant difference (P<0.05) between groups within the same microscope investigation; A, B, and C: different superscript capital letter in each raw means a significant difference (P<0.05) among the light and polarizing microscopes.

Table (6): Alterations in immunohistochemical expression of α-smooth muscle actin (α-SMA) and vimentin in ovary and oviducts among different groups (mean ± standard error).

	Organ	Groups				P value
		C1	HFD1	C2	HFD2	
α-SMA (%)	Ovary	3.00±0.13	6.88±0.35^{a}	3.76±0.11	21.98±1.54^{b,c}	P<0.01
	Oviduct	31.24±0.84	52.25±0.64^{a}	35.00±1.17	82.01±1.38^{b,c}	
Vimentin (%)	Ovary	8.31±0.35	13.76±0.49^{a}	9.81±0.38	28.82±1.72^{b,c}	
	Oviduct	20.49±0.53	54.59±0.99^{a}	22.20±0.42	92.58±7.10^{b,c}	

C1: control group "1"; C2: control group "2"; HFD1: high-fat diet group "1" treated for 6 weeks; HFD2: high-fat diet group "2" treated for 12 weeks; a: a significant increase when compared with C1 group; b: a significant increase when compared with C2 group; c: a significant increase when compared with HFD1 group.

In the current study, HFD consumption induced histopathological alterations, which then gradually increased to form fibrosis in time-dependent manner in both ovary and oviduct. Few researches are available regarding the impact of HFD on the ovarian and oviduct tissues. In this regard, accumulated evidence suggests that HFD consumption causes histopathological alteration in the ovarian and oviduct tissues including cytoplasmic vaculation, marked thickness of the oviduct walls and the mucosal stromal layer appeared more loosely arranged, decreased number of primordial follicles with an increase of the number of primary, secondary, and tertiary follicles, as well as increased cortex/medulla ratio, corpus luteum development, and PCOS. Moreover, HFD ingestion increased the number of atretic follicles through triggering follicular and granulosa cells apoptosis[11,12,29]. Therefore, Hilal *et al*.[12] suggested that HFD induces follicular maturation, which accelerates the rate of follicular loss by decreasing the number of primordial follicles. Huge fat droplets developed in the stromal layers of the ovary and oviducts as a result of the HFD ingestion, and their histological integrity was significantly changed. Hyper-proliferative uterus, vacuolated ovarian tissue, and thicker oviduct walls were among the modifications[29]. HFD consumption was reported to cause impaired puberty and disrupted estrous cycle, and decreased fertility rates[11]. Several authors attributed the pathological impact of HFD on the ovary and oviducts to the inflammatory

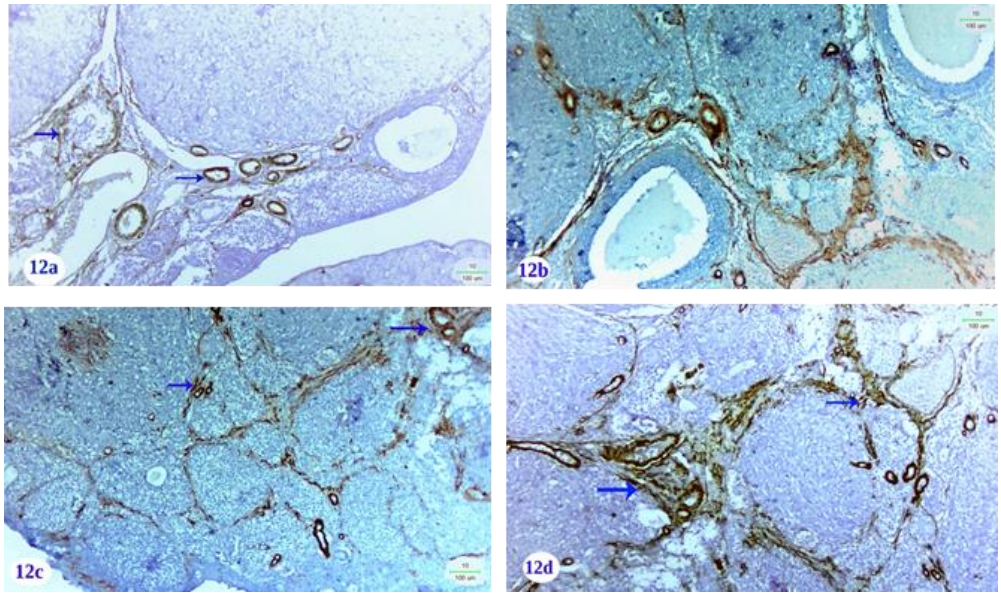

Figure (12): Alteration in α-smooth muscle actin (α-SMA) immunoexpression in ovarian tissues (α-SMA immunostain; scale bar: 100 µm). **(a)** Section in ovary of a control rat showing scanty expression of α-SMA around blood vessels and follicles (brown color). **(b)** Section in ovary of a rat from high-fat diet group "1" (HDF1) group showing moderate immunoreactivity of α-SMA in ovarian tissue. **(c)** Section in control rat from C2 group showing weak α-SMA immunoreactivity. **(d)** Section in ovary of a rat from HFD2 group showing strong immunoexpression of α-SMA.

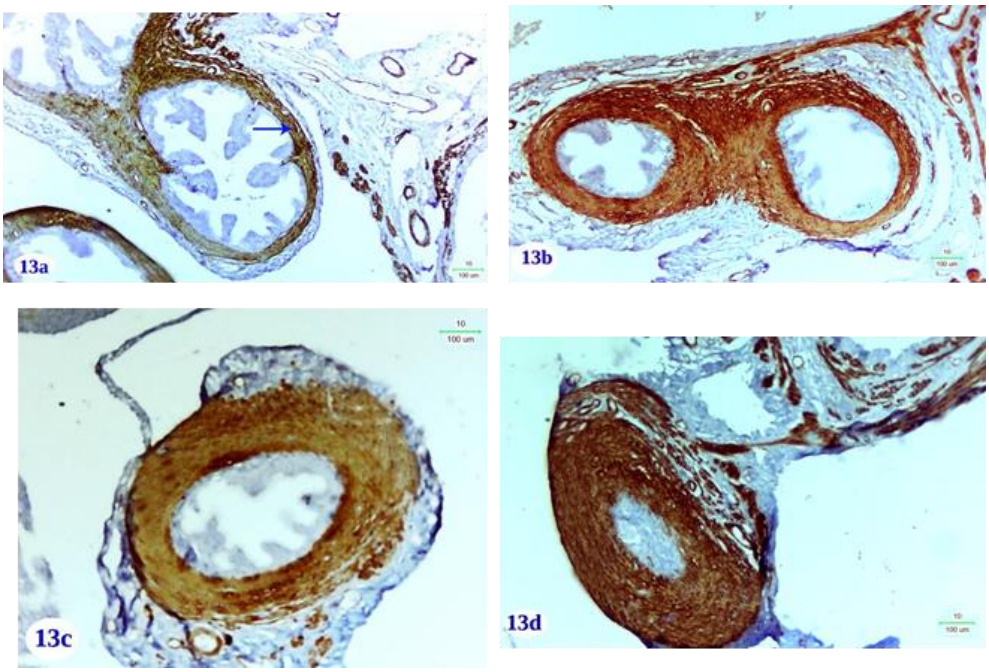

Figure (13): Alteration in α-smooth muscle actin (α-SMA) immunoexpression in oviducts (α-SMA immunostain; **scale bar:** 100 µm). **(a and c)** Sections in oviduct of control rats from c1 and c2 groups, respectively showing regular immunoreactivity of α-SMA in muscularis layer and around blood vessels (brown color). **(b)** Section in oviduct of a rat from high-fat diet group "1" (HDF1) group showing strong immunoreactivity of α-SMA in oviduct wall. **(d)** Section in oviduct of a rat from HFD2 group showing strong immunoexpression of α-SMA.

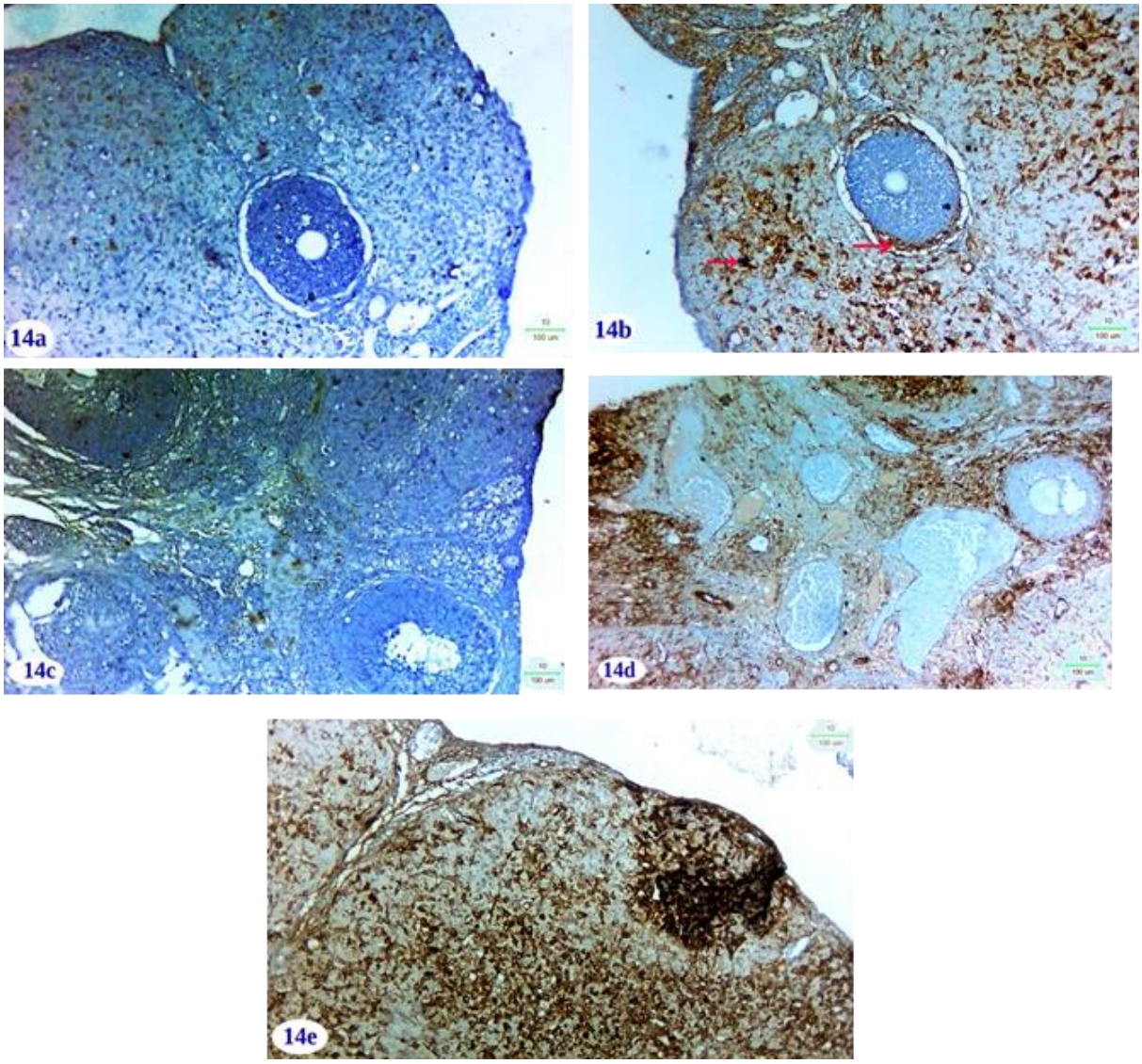

Figure (14): Alteration in vimentin immunoexpression in ovarian tissues (vimentin immunostain; scale bar: 100 µm). **(a)** Section in ovary of a control rat showing weak immunoreaction of vimentin (brown color). **(b)** Section in ovary of a rat from high-fat diet group "1" (HDF1) group showing considerable immunoreactivity of vimentin. **(c)** Section in control rat from C2 group showing weak vimentin immunoreactivity in ovarian cortex and medulla. **(d and e)** Sections in ovaries of rats from HFD2 group showing strong immunoexpression of vimentin.

effects[14,29,30]. The impact of HFD on inflammatory status in the ovary and oviduct in mice was reported[29], as HFD was found to increase significantly the expression levels of interleukin-6 (IL-6) and TNF-α. The HFD-induced adipose tissue plays as a dynamic endocrine organ, which can secrete a variety of pro-inflammatory cytokines including IL-6 and TNF-α. Furthermore, obesity can be considered as a low-grade chronic inflammatory status, and proinflammatory cytokines as TNF-α, IL-1, and IL-6 are considered as biomarkers of this condition[29,30]. The immunological environment within the lumen of the oviduct is maintained by the mucosal layer. Chronic inflammation can cause oviduct mucosal injury and immunological malfunction, causing infertility, early pregnancy abortion, ectopic pregnancy, and even tumors, in addition to diminished reproductive capacities[1].

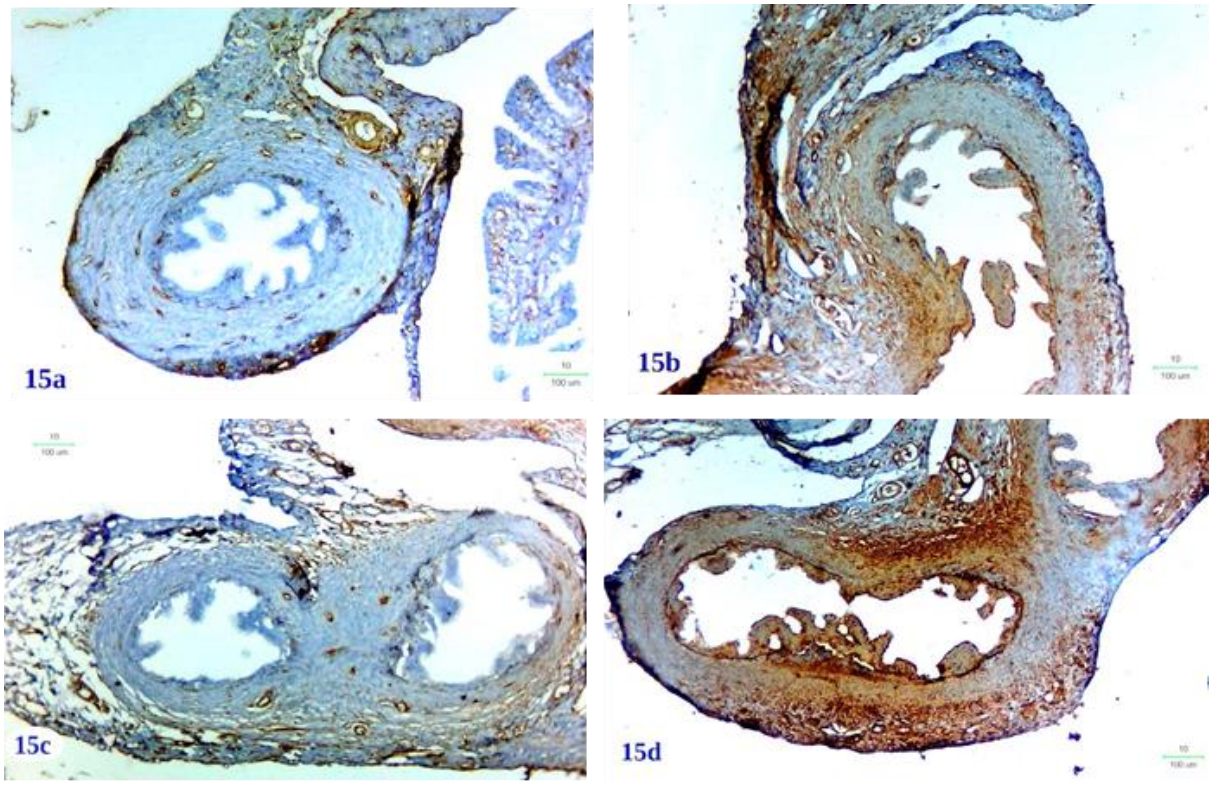

Figure (15): Alteration in vimentin immunoexpression in oviducts (vimentin immunostain; scale bar: 100 µm). **(a and c)** Sections in oviduct of control rats from c1 and c2 groups, respectively, showing regular immunoreactivity of vimentin in muscularis layer and around blood vessels (brown color). **(b)** Section in oviduct of a rat from high-fat diet group "1" (HDF1) group showing strong immunoreactivity of vimentin in oviduct wall. **(d)** Section in oviduct of a rat from HFD2 group showing strong immunoexpression of vimentin.

Our results showed that HFD consumption induced fibrosis in ovary and oviduct, which represented by significant increase of hydroxyproline and collagen fibers (demonstrated *via* histological stains as MT, PSR, and VG) in addition to immunohistochemical over-expression of vimentin and α-SMA in both ovary and oviducts. Our finding can be confirmed by several studies that reported the fibrotic impact of HFD on different organs including liver[31], Kidney[32], Lung[33], and Heart[34].

Ovarian fibrosis, however, has received little attention either worldwide or nationally. Ovarian follicles, the functional units of the ovary, develop in a complex micro-environment that composed of extracellular matrix (ECM) molecules, smooth muscle cells, fibroblasts, neurons, immunological cells and endothelial cells. The ovarian stromal ECM develops in interstitial collagen type I, III, and IV in tunica albuginea, as well as, glycoproteins, and proteoglycans[7,35]. During ovulation, follicular collagen fibers are altered because of the pre-ovulatory increase of collagenolytic activities, which support ovaries structural strength and provide the ECM in which follicular maturation, ovulation, and development of corpus luteum occurs[35]. During follicular development, the stromal cells proliferate and differentiate to inner thecal cells that maintain the follicular structure and integrity, and to outer myofibroblast that responsible of ECM secretion[36].

Ovarian fibrosis is closely related to hyperactivity of myofibroblasts, which effectively secretes large amounts of ECM[36], as well as, a remarkable number of molecular factors are required for

ECM formation including vascular endothelial growth factor (VEGF), matrix metalloproteinases (MMPs), peroxisome proliferator-activated receptor gamma (PPAR-γ), tissue inhibitors of matrix metalloproteinases (TIMPs), transforming growth factor‑beta 1 (TGF-β1), connective tissue growth factor (CTGF), and endothelin-1 (ET-1)[5]. The main histo-pathological features of ovarian fibrosis are the thick capsule, proliferated mesenchymal connective tissue, abnormal proliferation of fibroblasts, a thickened layer of theca cells, and reduction or absence of ovarian follicles[5,10]. Fibrosis progression was found to be associated with chronic inflammation in different tissues, and most chronic fibrotic changes have a persistent irritant that promotes fibrogenic cytokines and connective tissue deposition, altering the normal tissue structure[9]. Several studies have demonstrated the effects of low chronic inflammation rates on the development of PCOS associated fibrosis[35]. It was found that with increased reproductive age, ovarian fibrosis resulted from the accumulation of type I and III collagen[7]. Ovarian fibrosis in the stroma and tunica albuginea causes abnormal ovulation[9]. Oviduct fibrosis is induced due to inflammatory processes and massive inflammatory cell infiltration; induced oviduct cell damage in rats and mares has been reported[37,38]. Fibrotic occlusion of the oviduct occurred because of infection with *Chlamydia muridarum* in murine model and in human fallopian tube[39]. Quinacrine was found to induce occlusive fibrosis in the fallopian tube as a result of a distinct inflammatory response with marked increase of pro-inflammatory and pro-fibrotic cytokine including TNF-α and IL-1β[40]. Furthermore, TNF-α can accelerate the progression of fibrosis[41]. The ECM of the oviducts is subject to several alterations due to hormonal influences and aging[16]. Electron microscopy showed alterations in the architecture of connective tissue framework of the oviducts including thickness of basal membrane, greater deposits of collagen, as the glycoprotein expression increased due to the aging[16]. Based on real time polymerase chain reaction (qPCR) and histological PSR staining of collagen I and collagen III proteins, the presence of these two types of fibers in all regions of the oviduct was demonstrated in mares' oviducts in all ages[38]. Collagen I was more expressed than collagen III in all portions of the oviduct, mainly in the oldest mares, while collagen III mRNA transcripts were higher in the youngest mares[38]. However, there is a lack of studies regarding oviduct fibrosis. The current immunohistochemical findings revealed a significant increase of vimentin and α-SMA along with ovarian and oviduct fibrosis. Several studies considered vimentin and α-SMA as reliable fibrotic markers[42-44]. Mesenchymal myofibroblasts cells have an intermediate nature between fibroblasts and smooth muscle cells and they are the major cells responsible for the production of collagen, which leads to fibrosis. Immuno-histochemically, myofibroblasts were found to express vimentin and α-SMA in varying amounts during the development, and in fibrosis[42]. Vimentin is strongly expressed in mesenchyme tissues, with weak to negative immunoexpression in epithelial cells, whereas α-SMA expression in the cytoplasm provides cellular contractility, which is intimately related with fibrosis[44]. Myofibroblasts generally vanish following effective tissue healing, but deregulation of normal repair mechanisms, such as chronic inflammation or oxidative stress in the tissue, can result in prolonged myo-fibroblasts activation leading to excess collagen production, which finally results in fibrosis[43]. The significant increase of hydroxyproline, a major component of collagen, in the presented work is in agreement with several studies that reported the correlation between fibrosis and hydroxyproline elevation[43,45]. A Hydroxy-proline value is a surrogate indicator of collagen regulation and metabolism. Proline hydroxylation permits the collagen helix to twist sharply and stabilizes its structure. Increased hydroxyproline levels represent

elevated collagen levels and are demonstrated in fibrotic diseases[6].

Under our experimental conditions, in ovarian and oviduct fibrosis, PSR stain was found to be the best staining procedure for revealing the presence, describing the distribution patterns, and performing quantitative estimation of collagen fibers, as well as for clearly appreciating the thinnest fibers and networks within the tunica muscularis in oviducts. However, PSR presented significant increase in collagenous contents when compared with MT and VG stains. Our findings are in agreement with those of Segnani *et al*.[46], who reported that the VG technique only stained collagen fibers in the tunica mucosa and submucosa, whereas Sirius red staining revealed collagen fibers all over the wall, highlighting the thin collagen network in between the muscle compartment. Because they rely on differential binding by tissue components, VG and other trichrome stains as MT stain (which combine two or more anionic dyes) have been frequently regarded as specific for collagen fibers in tissues. Differences in the relative sizes of stains molecules, variations in the tissue physical structure (for example, tightly versus loosely packed), and differences in the amino acid content of tissue elements, all contribute to this differentiation. The VG and trichrome stains may not be ideal stain for identifying collagen due to their lack of precise selectivity. Furthermore, neither of these approaches is capable of detecting very fine collagen fibers, a drawback that might result in a significant underestimating of collagen content in some cases[47,48]. Therefore, the Picrosirius stain was proved to implement a more selective stain for demonstrating collagen fibers, which could be appreciated with less fading than VG stain and then observed considerably better using polarized light microscopy[46,49]. Because of its anisotropic molecular organization, collagen is birefringent and appears brilliant. The orderly binding of PSR stain molecules to collagen fiber further promotes collagen birefringence, resulting from the anisotropic molecular organization of PSR stain. Thus, the combination of PSR and polarized light microscopy provides an efficient way to demonstrate collagen fibers[50]. Collagen is divided into several subtypes, each having its own mechanical and organizational properties. Collagen's optical properties have been demonstrated to be influenced by its molecular organization, packing density, and ratio of subtypes[50].

Collagen birefringence has been reported to increase throughout time, implying the growth and maturity of collagen. The increased birefringence is attributable to higher collagen fiber alignment and packing, increased collagen molecular organization, and decreased interstitial ECM. In a somewhat loose network, the newly generated collagen subtype was of thinner Type III. Gradually, the relative amount of the thicker Type I collagen, which forms in a relatively tight network, was predominant and increased sharply[50-52]. The PSR stain is elongated birefringent molecules that, when bound within the upper groove of well oriented eosinophilic collagen molecules, the stains orient parallel to the long axis of each collagen fiber, causing considerably enhancing the normal birefringence stemming from a uniform fiber distribution[18]. Collagen can be demonstrated or quantified *via* several techniques including immunohistochemistry, confocal microscopy, polymerase chain reaction (PCR), and multiple histological staining approaches (MT, PSR, and VG stain). Even though the staining methods are not considered highly specific as the techniques mentioned, they can be quickly performed at a minimal cost. Thus, it is important to understand each stain's limits, as many special stains highlight collagen configuration and the heterogeneity of fibers direction in the tissues, with no differentiation between the types[27,48,49]. Polarized light microscopy is capable of non-destructively measuring of biological samples molecular organization in their native conditions. Moreover, polarized microscopy is very sensitive tool for

birefringence measurement, however, it can only image anisotropic structures that have a limited range of orientations with regarding to the microscope polarization axes. Thus, polarized light microscopy should be able to identify collagen fibers, as it is a highly ordered molecule and one of the most birefringent proteins in the tissue[53]. Birefringence is one of the many phenomena that can occur in anisotropic objects. When light passes through anisotropic structures, it is split into two beams with differing velocities and perpendicular vibration planes. Birefringence is a measurement of the difference in the refractive indices of two independent components (the fast ray and slow ray) of the incident ray passing through a sample. The samples that are analyzed with polarized light microscopy showed a complex mixture of different colors, revealing different collagen subtypes[18].

The special stain PSR is capable of enhancing the normal birefringence of the collagen during exposure to polarized light. In polarized light observation, thick fibrous collagen type I appears as bright yellow to orange, while thinner collagen type III, composed of reticular fiber, appears in green color[27]. Traditional polarized microscopes usually use Picrosirius staining, which intensifies the dichroism of collagen fibers reported to be 700%[24]. Keikhosravi *et al.*[53], reported the higher sensitivity of polarized microscopy compared to traditional microscopes as they observed 10-15 times increase in collagen dichroism enhancement in breast and pancreatic cancer tissues. Our findings of the present work are in agreement with those studies in that the sensitivity of polarized microscopy in quantifications of ovarian and oviducts fibrosis by comparing with traditional light microscope. In conclusion, our work concluded that: (1) Chronic consumption of HFD induced fibrosis in ovary and oviducts. (2) Under our experimental conditions, PSR stain is the best method for further investigation and demonstration of ovarian and oviduct fibrosis, with using either traditional light or polarizing microscopes when compared with MT and VG stains. (3) Our work can recommend polarizing microscope as a tool to evaluate fibrosis of ovary and oviducts, as it is a cheap, less bulky, and user friendly tool. (4) Polarizing microscope can differentiate between different collagen patterns, as mature thick type I collagen appeared with orange to red color, while thin immature collagen type III was green in color. However, studies are still needed to be able to recommend polarizing microscopy for demonstrating of fibrosis in different organs.

FUNDING SOURCE DISCLOSURE

This study did not receive any specific grant from funding agencies in the public, commercial, or not-for-profit sectors.

CONFLICT OF INTEREST

There is no conflict of interest.

REFERENCES

[1] Li, K.; Zhao, J.; Wang, M. *et al.* (2021). The roles of various prostaglandins in fibrosis: a review. Biomolecules, 11(6): 789 (DOI: 10.3390/biom11060789).

[2] Wu, M.; Xu, H.; Liu, J. *et al.* (2021). Metformin and fibrosis: a review of existing evidence and mechanisms. J Diabetes Res, 2021: 6673525 (DOI: 10.1155/2021/6673525).

[3] Zhang, W.-J.; Chen, S.-J.; Zhou, S.-C. *et al.* (2021). Inflammasomes and fibrosis. Front Immunol, 12: 643149 (DOI: 10.3389/fimmu.2021. 643149).

[4] Liedtke, C.; Nevzorova, Y. A.; Luedde, T. *et al.* (2022). Liver fibrosis-from mechanisms of injury to modulation of disease. Front Med, 8: 814496 (DOI: 10.3389/fmed.2021. 814496).

[5] Zhou, F.; Shi, L.-B. and Zhang, S.-Y. (2017). Ovarian fibrosis: a phenomenon of concern. Chin Med J (Engl), 130(3): 365-371.

[6] Briley, S. M.; Jasti, S.; McCracken, J. M. *et al.* (2016). Reproductive age-associated fibrosis in the stroma of the mammalian ovary. Reproduction, 152(3): 245-260.

[7] Parkes, W. S.; Amargant, F.; Zhou, L. T. *et al.* (2021). Hyaluronan and collagen are prominent extracellular matrix components in bovine and porcine ovaries. Genes, 12(8): 1186 (DOI: 10.3390/genes12081186).

[8] Pilling, D.; Karhadkar, T. R. and Gomer, R. H. (2021). High-fat diet-induced adipose tissue and liver inflammation and steatosis in mice are reduced by inhibiting sialidases. Am J Pathol, 191: 131-143.

[9] Landry, D. A.; Vaishnav, H. T. and Vanderhyden, B. C. (2020). The significance of ovarian fibrosis. Oncotarget, 11(47): 4366-4370.

[10] Wang, D.; Wang, W.; Liang, Q. *et al.* (2018). DHEA-induced ovarian hyperfibrosis is mediated by TGF-β signaling pathway. J Ovarian Res, 11: 6 (DOI: 10.1186/s13048-017-0375-7).

[11] Zhou, Z.; Lin, Q.; Xu, X. *et al*. (2019). Maternal high-fat diet impairs follicular development of offspring through intraovarian kisspeptin/GPR54 system. Reprod Biol Endocrinol, 17: 13 (DOI: 10.1186/s12958-019-0457-z).

[12] Hilal, G.; Fatma, T.; Ferruh, Y. *et al.* (2020). Effect of high-fat diet on the various morphological parameters of the ovary. Anat Cell Biol, 53: 58-67.

[13] Hussain, A.; Cho, J. S.; Kim, J.-S. *et al.* (2021). Protective effects of polyphenol enriched complex plants extract on metabolic dysfunctions associated with obesity and related nonalcoholic fatty liver diseases in high fat diet-induced C57BL/6 mice. Molecules, 26(2): 302 (DOI: 10.3390/molecules26020302).

[14] Begum, N.; Manipriya, K. and Veeresh, B. (2022). Role of high-fat diet on letrozole-induced polycystic ovarian syndrome in rats. Eur J Pharmacol, 917: 174746 (DOI: 10.1016/j.ejphar.2022.174746).

[15] Ramakrishnan, S.; Kunjunni, K. T. and Varghese S. (2021). A comparative study on segmental micro-anatomy of the human fallopian tube. Natl J Clin Anat, 2021; 10: 46-50.

[16] Souza, C. F. C.; Pires, L. A. S.; Babinski, M. D. D. *et al*. (2021). Organization of the fibrous connective tissue of the fallopian tubes in fertile and climacteric periods: a scanning electron microscopic and stereologic study. Int J Clin Exp Pathol, 14(9): 956-963.

[17] Cabibi, D.; Bronte, F.; Porcasi, R. *et al.* (2015). Comparison of histo-chemical stainings in evaluation of liver fibrosis and correlation with transient elastography in chronic hepatitis. Anal Cell Pathol (Amst), 2015: 431750 (DOI: 10.1155/2015/431750).

[18] Liu, J.; Xu, M.-Y.; Wu, J. *et al.* (2021). Picrosirius-polarization method for collagen fiber detection in tendons: a mini-review. Orthop Surg, 13(3): 701-707.

[19] Zimmermann, E.; Mukherjee, S. S.; Falahkheirkhah, K. *et al.* (2021). Detection and quantification of myocardial fibrosis using stain-free infrared spectroscopic imaging. Arch Pathol Lab Med, 145(12): 1526-1535.

[20] Elsisy, R. A.; Abu El-Magd, M. and Abdelkarim, M. A. (2021). High-fructose diet induces earlier and more severe kidney damage than high-fat diet on rats. Egypt J Histol, 44(2): 535-544.

[21] Reddy, G. K. and Enwemeka, C. S. (1996). A simplified method for the analysis of hydroxyproline in biological tissues. Clin Biochem, 29(3): 225-229.

[22] Bancroft, J. D. and Layton, C. (2013) The Hematoxylin and Eosin. In: Bancroft's Theory and Practice of Histological Techniques (Suvarna, S. K., Layton, C. and Bancroft, J. D., eds),

7th Edition, pp. 172-214. Elsevier-Churchill Livingstone, Philadelphia, PA, USA.

[23] Drury, R. A. B. and Wallington, E. A. (1980). Carleton's Histological Technique, 5th Edition. Oxford University Press, Oxiford, UK.

[24] Junqueira, L. C.; Bignolas, G. and Brentani, R. R. (1979). Picrosirius staining plus polarization microscopy, a specific method for collagen detection in tissue sections. Histochem J, 11(4): 447-455.

[25] Bancroft, J. D. and Cook, H. C. (1984). Manual of Histological Techniques. Churchill Livingstone, New York, NY, USA.

[26] Ramos-Vara, J. A.; Kiupel, M.; Baszler, T. *et al.* (2008). Suggested guidelines for immunohistochemical techniques in veterinary diagnostic laboratories. J Vet Diagn Invest, 20(4): 393-413.

[27] Coelho, P. G. B.; de Souza, M. V.; Conceição, L. G. *et al.* (2018). Evaluation of dermal collagen stained with Picrosirius red and examined under polarized light microscopy. An Bras Dermatol, 93(3): 415-418.

[28] Steel, R. G. D.; Torrie, J. H. and Dickey, D. A. (1997): Principles and procedures of Statistics: A Biometrical Approach. McGraw-Hill, New York, NY, USA.

[29] Gao, X.; Li, Y.; Ma, Z.; *et al.* (2021). Obesity induces morphological and functional changes in female reproductive system through increases in NF-κB and MAPK signaling in mice. Reprod Biol Endocrinol, 19: 148 (DOI: 10.1186/s12958-021-00833-x).

[30] Shen, H.-R.; Xu, X.; and Li, X.-L. (2021). Berberine exerts a protective effect on rats with polycystic ovary syndrome by inhibiting the inflammatory response and cell apoptosis. Reprod Biol Endocrinol, 19: 3 (DOI: 10.1186/s12958-020-00684-y).

[31] Xin, X.; Cai, B. Y.; Chen, C. *et al.* (2020). High-trans fatty acid and high-sugar diets can cause mice with non-alcoholic steatohepatitis with liver fibrosis and potential pathogenesis. Nutr Metab (Lond), 17: 40 (DOI: 10.1186/s12986-020-00462-y).

[32] Liu, K.; Zhou, S.; Liu, J. *et al.* (2019). Silibinin attenuates high-fat diet-induced renal fibrosis of diabetic nephropathy. Drug Des Devel Ther, 13: 3117-3126.

[33] Hegab, A. E.; Ozaki, M.; Kagawa, S. *et al.* (2021). Effect of high fat diet on the severity and repair of lung fibrosis in mice. Stem Cells Dev, 30(18): 908-921.

[34] Czarzasta, K.; Koperski, Ł.; Fus, Ł. *et al.* (2018). The effects of a high-fat diet on left ventricular fibrosis. Kardiol Pol, 76(4): 802-804.

[35] Bulut, G.; Kurdoglu, Z.; Dönmez, Y. B. *et al.* (2015). Effects of jnk inhibitor on inflammation and fibrosis in the ovary tissue of a rat model of polycystic ovary syndrome. Int J Clin Exp Pathol, 8(8): 8774-8785.

[36] Cui, L.; Bao, H.; Liu, Z. *et al.* (2020). hUMSCs regulate the differentiation of ovarian stromal cells *via* TGF-β1/Smad3 signaling pathway to inhibit ovarian fibrosis to repair ovarian function in POI rats. Stem Cell Res Ther, 11: 386 (DOI: 10.1186/s13287-020-01904-3.

[37] Yang, J.; Chi, C.; Liu, Z. *et al.* (2015). Ultrastructure damage of oviduct telocytes in rat model of acute salpingitis. J Cell Mol Med, 19(7): 1720-1728.

[38] Pinto-Bravo P., Rebordão M. R., Amaral A. *et al.* (2018). Is mare endometrosis linked to oviduct fibrosis? Pferdeheilkunde-Equine Medicine, 34: 43-46.

[39] Shah, A. A.; Schripsema, J. H.; Imtiaz, M. T. *et al.* (2005). Histopathologic changes related to fibrotic oviduct occlusion after genital tract infection of mice with *Chlamydia muridarum*. Sex Transm Dis, 32: 49-56.

[40] Growe, R. G.; Luster, M. I.; Fail, P. A. *et al.* (2013). Quinacrine-induced occlusive fibrosis in the human fallopian tube is due to a unique inflammatory response and modification of repair mechanisms. J Reprod Immunol., 97(2): 159-166.

[41] Saha, P. and Smith, A. (2018): TNF-α (tumor necrosis factor-α): a paradox in Thrombosis. Arterioscler Thromb Vasc Biol, 38(11): 2542-2543.

[42] Hashimoto, A.; Karim, M. R.; Kuramochi, M. *et al.* (2020). Characterization of macrophages and myofibroblasts appearing in dibutyltin dichloride-induced rat pancreatic fibrosis. Toxicol Pathol., 48(3): 509-523.

[43] Xu, C.; Bao, M.; Fan, X. *et al.* (2022). EndMT: new findings on the origin of myofibroblasts in endometrial fibrosis of intrauterine adhesions. Reprod Biol Endocrinol, 20: 9 (DOI: 10.1186/s12958-022-00887-5).

[44] Xu, Y.; Peng, W.; Han, D. *et al.* (2021). Maiwei Yangfei decoction prevents bleomycin-induced pulmonary fibrosis in mice. Exp Ther Med, 22(5): 1306 (DOI: 10.3892/etm.2021.10741).

[45] Ahmed, R. A. (2017). Histological assessment and quantification of hypervitaminosis A-induced fibrosis in liver, kidney and testis of albino rats. World J Pharm Sci, 5(8): 209-220.

[46] Segnani, C.; Ippolito, C.; Antonioli, L. *et al.* (2015). Histochemical detection of collagen fibers by Sirius red/fast green is more sensitive than van Gieson or Sirius red alone in normal and inflamed rat colon. PloS one, 10(12): e0144630 (DOI: 10.1371/journal.pone.0144630).

[47] Kiernan J. A (2015). Methods for Connective Tissue. In: Histological and Histochemical Methods: Theory and Practice (Kiernan J. A, ed), 5th Edition, pp. 184-205. Scion Publishing Ltd, Oxford, UK.

[48] Rich, L. and Whittaker, P. (2005). Collagen and Picrosirius red staining: a polarized light assessment of fibrillar hue and spatial distribution. Braz J Morphol Sci; 22(2): 97-104.

[49] Sweat, F.; Puchtler, H. and Rosenthal, S. I. (1964). Sirius red F3ba as a stain for connective tissue. Arch Pathol, 78: 69-72.

[50] Zhang, H.; Sun, L.; Wang, W. *et al.* (2006). Quantitative analysis of fibrosis formation on the microcapsule surface with the use of Picro-Sirius red staining, polarized light microscopy, and digital image analysis. J Biomed Mater Res, Part A, 76: 120-125.

[51] Montes, G. S. and Junqueira, L. C. (1991). The use of the Picrosirius-polarization method for the study of the biopathology of collagen. Mem Inst Oswaldo Cruz, 86 (suppl 3): 1-11.

[52] Gay, S. and Gay, R.E. (1992). Connective Tissue Structure and Function. In: Cecil Textbook of Medicine (Wyngaarden J. B., Smith L. H. Jr, Bennett J. C., eds), pp. 1491-1496. WB Saunders, Philadelphia, PA, USA.

[53] Keikhosravi, A.; Liu, Y.; Drifka, C. *et al.* (2017). Quantification of collagen organization in histopathology samples using liquid crystal based polarization microscopy. Biomed Opt Express, 8(9): 4243-4256.

How to cite this article:
Ahmed, R. A. (2023). Differential staining patterns for evaluation of ovarian and oviducts fibrosis using the polarized light microscope and the digital images analysis. Egyptian Journal of Zoology, 79: 1-28 (DOI: 10.21608/ejz.2022.134076.1080).

أنماط الصِبَغ التفاضلية لتقييم تليف المبيض وقنوات البيض باستخدام المجهر الضوئي المستقطب وتحليل الصور الرقمية

رانيا عبد الكريم إبراهيم أحمد

قسم علم الحيوان، كلية العلوم، جامعة السويس، السويس، مصر

تستخدام العديد من التقنيات النسيجية والكيمياء المناعية النسيجية في تشخيص التليف وذلك للحصول على تصور أفضل لأليات الكولاجين في كل من الأنسجة السوية والمرضية. وهناك حاجة إلى استحداث المزيد من الطرق البصرية. تهدف الدراسة الحالية إلى مقارنة كفاءة صبغات نسيجية متنوعة، باستخدام المجهر الضوئي التقليدي ومجهر الضوء المستقطب، لتحديد وتقييم تليف المبيض وقنوات البيض الناجم عن النظام الغذائي عالي الدهون. تم توزيع "24" من إناث الجِرذان المهقاء (*Rattus norvegicus albinus*) عشوائيًا إلى "4" مجموعات (6 جِرذ/مجموعة): المجموعتين الضابطتين (تم تغذيتهما على النظام الغذائي القياسي لمدة 6 و 12 أسبوع)، والمجموعة التي تم تغذيتها على النظام الغذائي عالي الدهون لمدة 6 أسابيع، والمجموعة التي تم تغذيتها على النظام الغذائي عالي الدهون لمدة 12 أسبوع. تم فحص تليف المبيض وقناة البيض من خلال عدة صبغات نسيجية تشمل صبغات الهيماتوكسيلين والإيوسين، وبيكروسيرس الأحمر، وفان جيسون، وماسون ثلاثي الكروم، باستخدام المجهر الضوئي التقليدي والمجهر الضوئي المستقطب، بالإضافة إلى تقييم التعبير الكيمياء المناعي النسيجي لكل من "α-SMA" والفيمنتين. تم أيضا قياس الهيدروكسي برولين وعامل تنكرز الورم-ألفا بطرق بيوكيميائية في الأنسجة. وقد أظهرت النتائج أن النظام الغذائي عالي الدهون تسبب في تليف المبيض وقناة البيض بمعدل يتزايد مع طول مدة المعاملة، صحب ذلك زيادات ذات دلالة إحصائية في قيم كل من الهيدروكسي برولين وعامل تنكرز الورم-ألفا، و "α-SMA" والفيمنتين. وحققت صبغة بيكروسيريس الأحمر نتائج مثالية في إظهار الكولاجين بالمقارنة مع صبغات فان جيسون، وماسون ثلاثي الكروم. كما حققت صبغة بيكروسيريس الأحمر مع المجهر المستقطب حساسية عالية في تقدير ألياف الكولاجين مقارنة بالمجهر الضوئي التقليدي. وتوصي الدراسة الحالية باستخدام المجهر المستقطب كأداة لتقييم تليف المبيض وقنوات البيض.